Surface Plasmon Resonance (SPR) Bio-Sensors to Detect Target Molecules in Undiluted

Human Serum

by

Ran Wang

A Dissertation Presented in Partial Fulfillment
of the Requirements for the Degree
Doctor of Philosophy

Approved August 2015 by the
Graduate Supervisory Committee:

Junseok Chae, Chair
Bertan Bakkaloglu
Tsing Tsow
Michael Goryll

ARIZONA STATE UNIVERSITY

December 2015

ABSTRACT

Biosensors aiming at detection of target analytes, such as proteins, microbes, virus, and toxins, are widely needed for various applications including detection of chemical and biological warfare (CBW) agents, biomedicine, environmental monitoring, and drug screening. Surface Plasmon Resonance (SPR), as a surface-sensitive analytical tool, can very sensitively respond to minute changes of refractive index occurring adjacent to a metal film, offering detection limits up to a few ppt (pg/mL). Through SPR, the process of protein adsorption may be monitored in real-time, and transduced into an SPR angle shift. This unique technique bypasses the time-consuming, labor-intensive labeling processes, such as radioisotope and fluorescence labeling. More importantly, the method avoids the modification of the biomarker's characteristics and behaviors by labeling that often occurs in traditional biosensors. While many transducers, including SPR, offer high sensitivity, selectivity is determined by the bio-receptors. In traditional biosensors, the selectivity is provided by bio-receptors possessing highly specific binding affinity to capture target analytes, yet their use in biosensors are often limited by their relatively-weak binding affinity with analyte, non-specific adsorption, need for optimization conditions, low reproducibility, and difficulties integrating onto the surface of transducers. In order to circumvent the use of bio-receptors, the competitive adsorption of proteins, termed the Vroman effect, is utilized in this work. The Vroman effect was first reported by Vroman and Adams in 1969. The competitive adsorption targeted here occurs among different proteins competing to adsorb to a surface, when more than one type of protein is present. When lower-affinity proteins are adsorbed on the surface first, they can be displaced by higher-affinity proteins arriving at the surface at a later point in time. Moreover, only low-

i

affinity proteins can be displaced by high-affinity proteins, typically possessing higher molecular weight, yet the reverse sequence does not occur. The SPR biosensor based on competitive adsorption is successfully demonstrated to detect fibrinogen and thyroglobulin (Tg) in undiluted human serum and copper ions in drinking water through the denatured albumin.

ACKNOWLEDGMENTS

TABLE OF CONTENTS

LIST OF TABLES

LIST OF FIGURES

CHAPTER 1

INTRODUCTION

1.1 Sensitivity and Selectivity of Biosensors

A biosensor is an analytical device, used for the detection of a target biological analyte, which combines this target analyte with a physicochemical detector[1]. Extensive research efforts focus on developing a biosensor possessing both high selectivity and sensitivity[2].

Sensitivity is determined by transducers that convert the immobilization process to an alternate form of signal, such as an optical, mechanical, or electrical signal. Transducers may be broadly categorized as a labeled or label-free mechanism. The label-free mechanism is more frequently preferred over the labeled mechanism as the labeling process is time-consuming, labor-intensive, often difficult to achieve accurate quantification, and vulnerable to modifying target proteins characteristics and altering their behaviors[3,4]. Among various label-free mechanisms, SPR (Surface Plasmon Resonance) is a surface-sensitive analytical tool responding to minute changes in refractive index occurring adjacent to a metal film, offering detection limits up to few ppt (pg/mL). In this way, immobilization of proteins on the surface and their subsequent adsorption interactions may be monitored in real-time without labeling[5].

While many transducers, including SPR, offer high sensitivity, the low selectivity of these protein biosensors is a persistent challenge. Selectivity is determined by the bio-receptors, such as antibodies, protein lysates, lectins, peptides, and aptamers[6], which selectively capture target entities. However, these bio-receptors are often constrained by

their weak binding affinity with analytes, non-specific adsorption, low reproducibility, and difficulty with integration onto the transducer[7-9]. We utilize the competitive adsorption of proteins, which is a process driven by thermodynamics, to aim for a high selectivity for the SPR biosensor without the need for any bio-receptors. The competitive adsorption of proteins, termed the Vroman effect, was reported by Vroman and Adams in 1969[10], and many researchers have studied the Vroman effect since then[11-15]. The Vroman effect has been studied from many different aspects, including the adsorption from complex mixtures, protein sensing, the interplay of substrate surface to proteins, and the interaction artificial materials to the blood[7, 16, 17]. The competitive nature of protein adsorption onto the surface, primarily relies upon a protein's molecular weights[10]. Thus, low-molecular weight proteins are displaced by high-molecular weight proteins and/or more strongly interacting proteins.

1.2 Applications of Biosensors

Biosensors are used in many areas such as medicine, biotechnology, environmental monitoring, food industry, and military technology[18]. According to various applications, biosensors aim at various target analytes, such as proteins, microbes, virus, and toxins. Our SPR biosensor is basically applied to detect proteins. Proteins are often targeted for detection as their relative and absolute levels of concentrations may be correlated to specific disease states and as such be used to assess the progress of disease and monitor the effects of treatment[18-21]. For the detection of heavy metal ions, native proteins can be used as bio-receptor to interact and combine with the heavy metal ions[22-25].

1.3 Competitive Adsorption of Proteins

In traditional biosensors, the selectivity is provided by bio-receptors possessing highly specific binding affinity to capture target analytes. There are many kinds of bio-receptors, such as antibodies, protein lysates, lectins, peptides, and aptamers, yet their use in biosensors are often limited by their relatively-weak binding affinity with analyte, non-specific adsorption, need for optimization conditions, low reproducibility, and difficulties integrating onto the surface of transducers[26, 27].

In order to circumvent the use of bio-receptors, we instead utilize the competitive adsorption of proteins, termed the Vroman effect. As shown in Figure 1.1, competitive adsorption relies on various interactions between proteins and surfaces. Different proteins may render different affinities to adsorb onto the same surface due to different sizes of proteins, as shown in Figure 1.1a. Proteins are biomolecules that are composed of amino acid subunits. Each amino acid has a side chain that gains or loses charge depending on the pH of the surrounding environment, as well as its own individual polar/nonpolar qualities. Charged regions can greatly contribute to how that protein interacts with other molecules and surfaces, as well as its own tertiary structure (protein folding). As a result of their hydrophilicity, charged amino acids tend to be located on the outside of proteins, where they are able to interact with surfaces. It is the unique combination of amino acids that gives a protein its properties. In terms of surface chemistry, protein adsorption is a critical phenomenon that describes the aggregation of these molecules on the exterior of a material. The tendency for proteins to remain attached to a surface depends largely on the material properties such as surface energy, texture, and relative charge distribution. Larger proteins are more likely to adsorb and remain attached to a surface due to the higher number of

3

contact sites between amino acids and the surface. The same protein may also render

different affinities to adsorb on different surfaces, as shown in Figure 1.1b. On protein

covered hydrophobic surface, proteins can anchor and then spread to realized binding, but

on protein covered hydrophilic surface, the binding fails, because the adsorption of proteins

on the top of pre-adsorbed protein monomers does not take place when the anchoring fails.
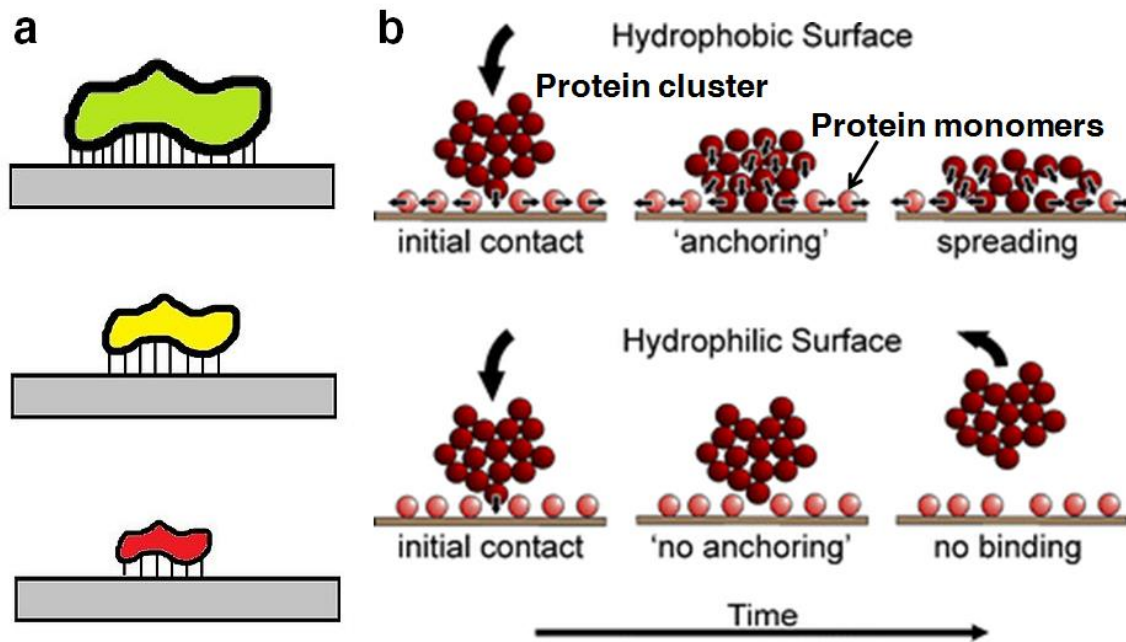
Figure 1.1 The principle of competitive adsorption of proteins (the Vroman effect). **a.** The effect of protein size on interaction with a surface. The larger proteins compose of more amino acids which is capable of making more interactions. **b.** Illustration of mechanism of the protein spreading process on protein monomers covered hydrophobic and hydrophilic surfaces.

Based on these nature characteristics of proteins, the competitive adsorption, as

shown in Figure 1.2, targeted here occurs among different proteins competing to adsorb to

a surface, when more than one type of protein is present. When lower-affinity proteins are

adsorbed onto the surface first, they can be displaced by higher-affinity proteins arriving

at the surface at a later point in time[28]. Moreover, only low-affinity proteins can be

displaced by high-affinity proteins, typically possessing higher molecular weight, yet the reverse sequence does not occur.
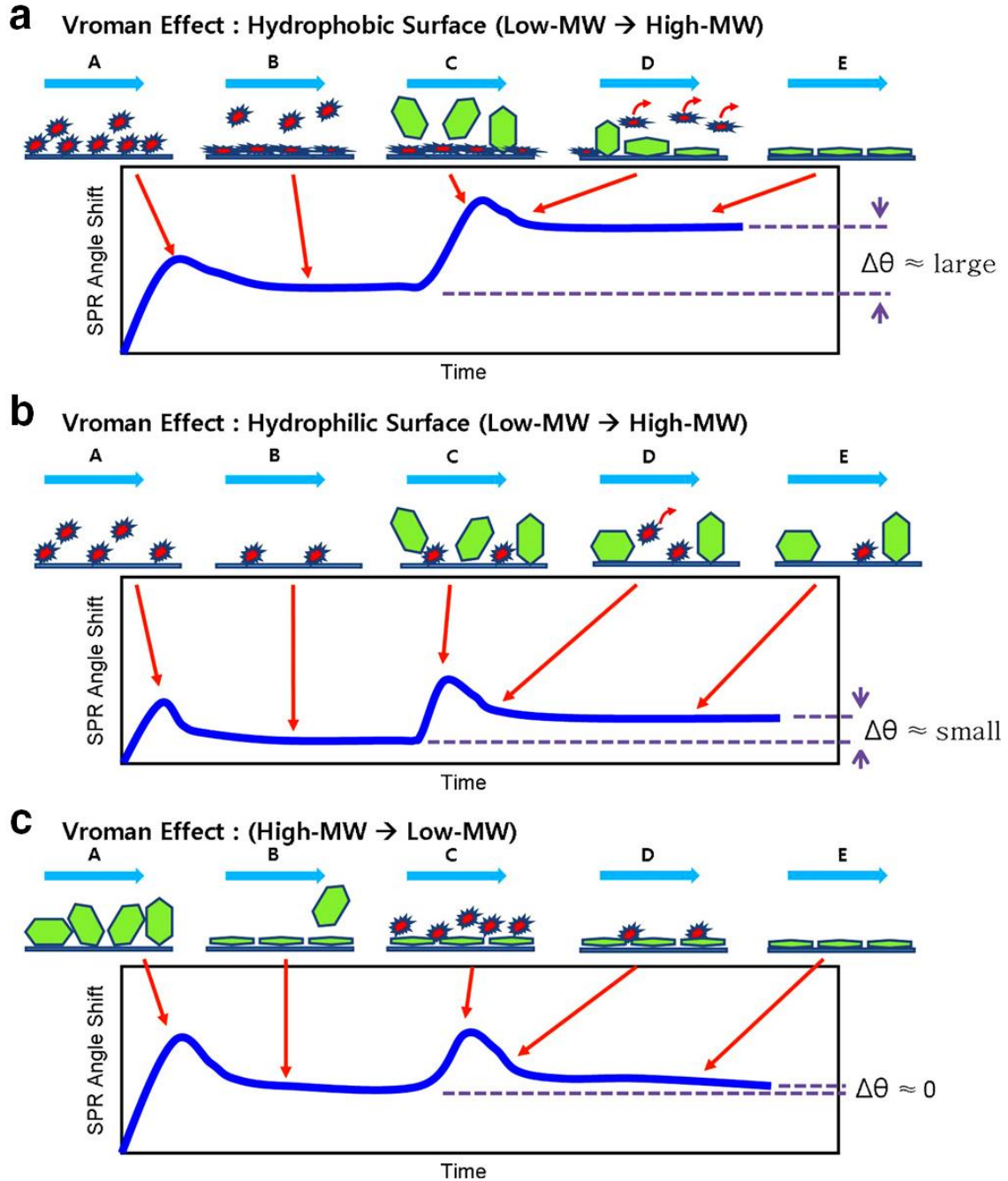
Figure 1.2 A schematic of SPR profiles and illustration of the Vroman effect. **a.** on the hydrophobic and **b.** the hydrophilic surfaces when the low molecular weight protein adsorbs first and then the high molecular weight protein arrives later to the surface. If the

high molecular weight protein adsorbs first and the low molecular weight protein comes later, then **c.** no angle change occurs.

The discovery and relevant studies of the Vroman effect has therived since 1969[10]. Brash, Ten Hove et al. studied fibrinogen adsorption from diluted plasma by adding I-fibrinogen as tracer protein to the plasma. Their results strongly indicate that conversion of fibrinogen, adsorbed from plasma to glass is owing to a displacement of this protein from the material surface with increasing contact time. Results of experiments, carried out by Elwing et al. and Poot et al., support the hypothesis that fibrinogen adsorbed from plasma to glass is displaced by high molecular weight kininogen (HMWK)[29, 30]. It has been suggested by Vroman that by diluting plasma sufficiently. The concentration of HMWK decreases to such a low value that adsorbed fibrinogen cannot be replaced anymore. This hypothesis is supported by the results of several authors who found that the adsorption of fibrinogen and several other proteins to various materials as a function of the plasma concentration shows a maximum at a plasma dilution of 1:100-1:1000. Both this plasma dilution effect and the above-mentioned displacement of fibrinogen are called the Vroman effect by Horbett. As suggested by Brash, the Vroman effect at the present moment more generally refers to sequential displacement of proteins adsorbing from plasma (or a mixture of proteins in solution) to a material surface[13].

Such transient adsorption can be understood from classical principles: from a mixture of an abundant component with low binding affinity and a scarce component with high binding affinity, the abundant component may first adsorb and then be gradually displaced by the scarce one. However, it has repeatedly been confirmed that dilution of a protein mixture may change the ratio of adsorbed quantities of different proteins and this

6

observation cannot be reconciled with classical binding theory. This phenomenon has shown that part of these effects can be qualitatively understood by assuming exponential relations between the second-order sorption rate constants and surface coverage. It has been demonstrated that by taking into account the space occupied by adsorbed protein molecules one may explain drastic effect on total surface coverage or adsorption kinetics. This concept is expanded by incorporation of surface diffusion and forces between adsorbed molecules. These aspects are integrated in a Monte Carlo simulation model with non-overlapping molecules. This model may explain qualitative differences observed in the adsorption of some specific proteins to phospholipid bilayers[12].

A standard depletion method of measuring adsorption was implemented using SDS-gel electrophoresis as a separation and quantification tool. The basic idea behind the depletion method is to measure solute (protein) concentration remaining in solution before-and-after contact with particulate materials bearing a surface chemistry of interest (hydrophobic octyl sepharose herein). The conclusion is that Brash and Lyman's idea that proteins adsorb in proportion to solution concentration was basically correct, except that mass balance mandates a discrimination against larger proteins adsorbing from a mixture of smaller-and larger proteins. This discrimination gives rise to a Vroman-like effect unrelated to adsorption kinetics or significant differences in protein affinity for hydrophobic surfaces[15].

Another study of Vroman effect is based on the observation that the strength of attachment of certain proteins to polymers (as measured by their resistance to detergent elution) increased with increasing residence time of the protein on the surface. Proteins residing on the surface for days were less elutable with several different detergents than

those adsorbed for only a few hours. Blood plasma is used as the displacing agent to show that the attachment of fibrinogen to polyethylene, silicone rubber, and polystyrene grows stronger over a period of 1 h. Also, the rate which adsorbed fibrinogen molecules become undisplaceable by plasma differed on these materials. A model was developed to explain these results and was based on the postulate existence of two distinct types of adsorbed fibrinogen molecules. The model predicts the occurrence of maxima in fibrinogen adsorption from plasma as a function of contact time and plasma dilution, in accord with experimental observations. It is theorized that differences in the rate at which fibrinogen molecules become nondisplaceable can account for the differences in the Vroman effect observed on various materials[16].

Some other researches explain the mixing rules deriving from a relatively straightforward theory of protein adsorption that reveals how individual proteins comprising a mixture compete for space at a surface in the adsorption process. Reported results are specific to the liquid-vapor (LV) interface, a molecularly smooth hydrophobic surface where interfacial energetic can be directly and sensitively measured by tensiometric (surface thermodynamic) techniques. Insights into protein adsorption may thus be relevant to purely hydrophobic solid surfaces where dispersion force predominate, which probably do not directly extend to hydrophilic surfaces where more chemically specific interactions between proteins and the surface may occur. Using pendant-drop tensiometry, it is found that concentration-dependent interfacial tension of a broad array of purified human proteins spanning 3 decades in molecular weight are quite similar to one another and surprisingly similar to that of plasma and serum, when protein concentration is scaled on a weight/volume basis. These experimental outcomes are rationalized in terms of the mixing

8

model, as are adsorption-kinetic studies of binary mixtures that illuminate the cause of the Vroman effect[14].

Here, we utilize the competitive adsorption (the Vroman effect) to design the selectivity of detection primarily depending on proteins' affinity strength, and engineer surface characteristics, by changing the adsorption affinity according to the energy preference, in order to further increase selectivity[31].

1.4 SPR Biosensor

Because this sensing process occurs at the vicinity of the surface, it is appropriate to couple the process with a surface-sensitive analytical tool such as Surface Plasmon Resonance (SPR). SPR has merged as a powerful optical detection technique for setting label-free biomolecular interactions in real-time with variety of diverse applications, such as life science, electrochemistry, gas chemical vapor detection, food and environmental safety and beyond. SPR technology is commonly utilized for the study of molecular binding interactions between free analyte molecules in solution and designed sensing surfaces. SPR can very sensitively respond to minute changes of refractive index occurring adjacent to a gold film, offering detection limits up to a few ppt (pg/mL)[32, 33]. Through SPR, the process of competitive protein adsorption may be monitored in real-time[5], and transduced into an SPR angle shift. This unique technique bypasses the time-consuming, labor-intensive labeling processes, such as radioisotope and fluorescence labeling. More importantly, the method avoids the modification of the biomarker's characteristics and behaviors by labeling that often occurs in traditional biosensors[3, 4].

Figure 1.3 illustrates the principle of plasmon resonating on gold surface.

9
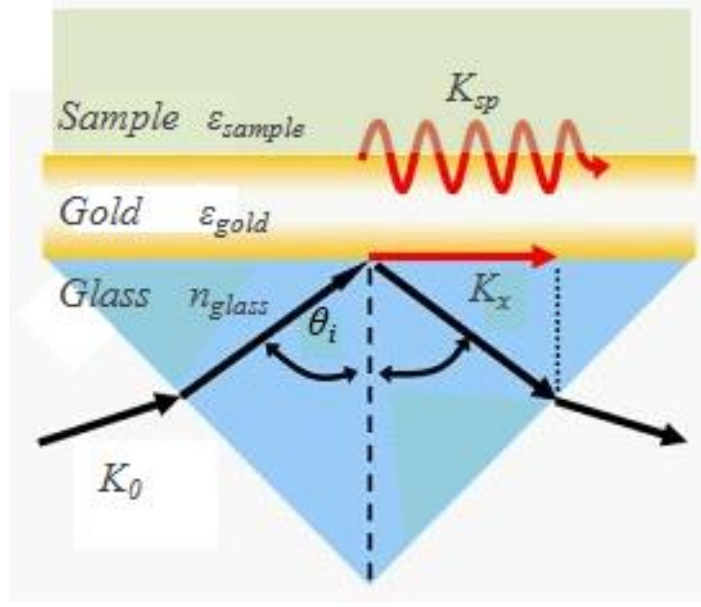
Figure 1.3 Schematic of surface plasmon resonance (SPR) angle derivation. The resonation of surface plasmons, as a function of dielectric constants of the gold and the sample medium (ε_{gold} and ε_{sample}), refractive index of the prism (n_{glass}), and the incident angle of the light (θ_i), appears as a dark band, and indicated by angle shift of the dip.

The propagation constant of the surface plasmon wave propagating at the interface between a dielectric and a gold film is given by

$$K_{sp} = K_0 \sqrt{\frac{\varepsilon_{gold}\varepsilon_{sample}}{\varepsilon_{gold} + \varepsilon_{sample}}} \, , \qquad\qquad 1.1$$

Where K_0 is the free space wave vector of the optical wave, ε_{gold} and ε_{sample} are the complex dielectric constants of the gold and the sample medium respectively. The enhanced wave vector of incident light (K_x) is given by

$$K_x = K_0 n_{glass} \sin\theta_i \, , \qquad\qquad 1.2$$

Where n_{glass} is the refractive index of the prism and θ_i is the angle of incidence. In order to excite the plasmons at resonance, the two vectors should be matched,

$$K_{sp} = K_x \, . \qquad\qquad 1.3$$

10

Therefore, a small variation of ε_{sample}, which is the dielectric properties of the medium adjacent to the sensing surface, will lead to a large change of SPR angle (θ_i).

SPR can be configured in various ways to monitor the molecular interactions. So far, there are three different optical systems to excite the resonation of surface plasmons, systems with prisms, grating and optical waveguides. Among them, SPR using a prism coupler is most widely adopted due to the enhanced simplicity, stability and sensitivity, which is called Kretschmann configuration. The SPR system consists of several components, including a light source, a prism, a sensing surface, biomolecules, a flow regulator, and a photodetector. Figure 1.4 shows a simple schematic of the SPR biosensor. A glass slide covered by a thin gold film is optically coupled to a prism via a refractive index matching liquid. Plane polarized light passes through a prism to the gold sensor chip over a wide range of incident angles and reflects from the back side of the sensor chip surface into a photodetector. At certain incident light angles, known as the resonance angle, light is absorbed by the electrons in the metal film of the sensor chip causing them to resonate. Simultaneously, a minimum in the intensity is observed, which appears as a dark band. These resonating electrons are sensitive to the surrounding environment. The result is the intensity loss in the reflected beam which can be seen as a dip in the SPR reflection intensity curve. The shape and the location of SPR dip can be used to interpret information about the sensing surface.
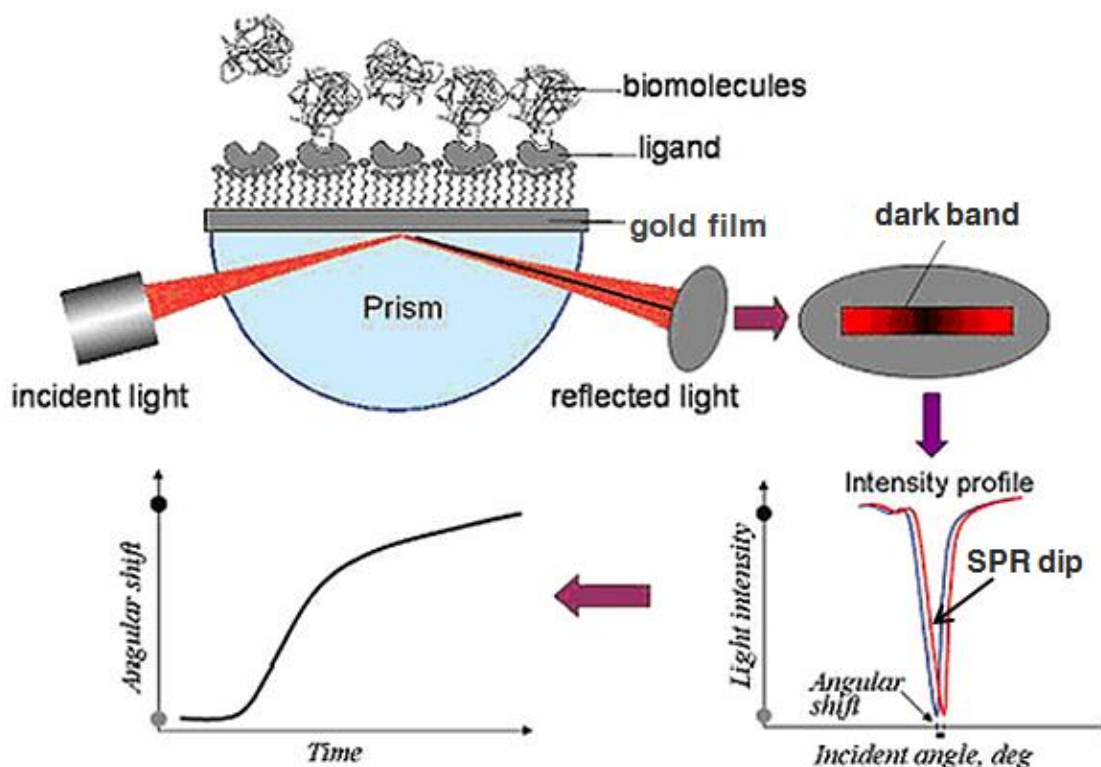
Figure 1.4 Schematic view of the surface plasmon resonance (SPR)-based biosensor. Any adsorption of biomolecules on the gold layer produces the SPR angle changes.

The immobilization of pre-adsorbed proteins on various sensing surfaces and the subsequent displacement process are quantitatively detected in a microfluidic integrated SPR biosensor. The microfluidic chip is capable of transporting a precise amount of biological samples to the detection areas to achieve highly sensitive and specific biosensing with decreased reaction time and less reagent consumption. Also the microfluidic system takes advantage of several intrinsic characteristics, including laminar flow, minimal handling of hazardous materials, multiple sample detections in parallel, portability and versatility in design[18].

12

1.5 Fabrication of the Sensing Surfaces

Glass slides (BK7, n=1.517, 150 μm thick, 18 x 18 mm) are first immersed in ethanol (Proof 200) and cleaned in an ultrasonic cleaner for 5 min. Subsequently, the slides are rinsed sequentially with ethanol and DI water, and dried by a N_2 stream. Cr is sputtered on the glass chips to a thickness of 2 nm followed by Au to a thickness of 47 nm. The slides are cleaned in a plasma cleaner at 10.15 W for 1 min[33].

To modify the bare gold chips with COOH-terminated SAM, the gold chips fabricated above are immersed in an ethanol (Proof 200) solution of alkane-thiols (1 mM) for 24 hours. Before use, they are rinsed with ethanol and dried by a N_2 stream. Compared with hydrophobic bare gold surfaces, COOH-SAM modified chips are hydrophilic, which leads to different interaction with proteins[34].

A glass slide having Cr/Au (2 nm/47 nm) is mounted on the SPR (BI-2000 from Biosensing Instrument Inc.). And then, a flow cell is coupled with the glass slide. Calibration of the SPR sensorgram is performed to minimize the discrepancy of sensitivity. The calibration coefficient, the ratio of the measured sensitivity to the theoretical sensitivity, is used to calibrate the SPR sensorgram.

60 μL of sample volume flows across the sensing surface for 2 mins (flow rate of 30 μL/min), which allows proteins having ample time to adsorb on the sensing surface before and after the PBS rinsing steps. All the data obtained from SPR measurements are under kinetic equilibrium.

CHAPTER 2

MEASUREMENT OF FIBRINOGEN IN UNDILUTED HUMAN SERUM

2.1 Introduction

Substantial evidence from epidemiological studies suggests that elevated plasma fibrinogen levels are associated with an increased risk of cardiovascular disorders, including ischemic heart disease (IHD), stroke and other thromboembolism[35, 36]. Currently deployed methods to measure fibrinogen can be classified into two groups: 'functional' and 'direct'. Functional methods measure the coagulation time of blood, which is proportional to the fibrinogen concentration. The most widely used method in functional fibrinogen assay in most clinical laboratories is the Clauss method, total clottable protein assay, which records the elapsed time to reach the coagulation end point. Direct methods quantify fibrinogen concentration directly, either immunologically, gravimetrically or by precipitation (by heat or salting out)[37, 38]. From dissimilar epidemiological studies that used different measure methods, the fibrinogen concentration in healthy individuals was identified to be in the range of 1.5 to 4.5 mg/mL. The fibrinogen concentration is dependent upon both genetic (intrinsic) and environmental (extrinsic) factors that include gender, age, body mass index and body habitus, metabolic syndrome, physical exercise, seasonal changes, vitamin C, infection, psychosocial factors, hormonal status, smoking and alcohol use[38].

Quantifying fibrinogen concentrations has been typically executed by a series of measurements with disposable sensor units[39]. However, variation occurs due to batch-to-batch irreproducibility and uncontrollable experimental conditions, which generates

14

unalterable false-positive/negative responses[40]. It is necessary to perform a series of measurements from a patient's blood sample to reduce these variations; this motivates our research to design a fibrinogen biosensor of having a regenerative sensing surface.

In this work, we present a regenerative fibrinogen biosensor using the competitive adsorption of proteins in a microfluidic environment. The target protein, fibrinogen, is adsorbed selectively on the sensing surface following the competitive process of protein adsorption/exchange. This adsorption and exchange process results in a refractive index change that is monitored by SPR. Figure 2.1 illustrates SPR sensorgram of the biosensor. A protein with relatively strong adsorption strength, IgM, is dominantly displaced by fibrinogen, yet is displaced much less significantly by other proteins in fibrinogen-spiked human serum samples[7]. Using the nature of competitive protein adsorption, we obviate the need to rely on complex assays and their attachment to transducers.
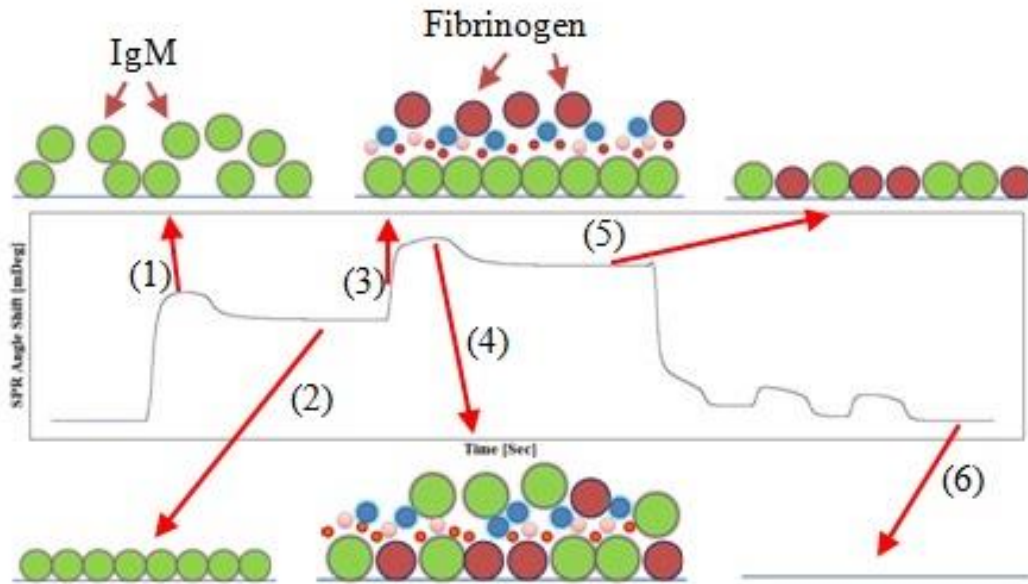
Figure 2.1 SPR angle profile of the competitive adsorption of proteins and regeneration of the sensing surface to measure fibrinogen in serum (1) injection of IgM to pre-adsorb on the surface (2) saturation of IgM and washing away of excess proteins (3) injection of

15

fibrinogen-spiked undiluted serum sample (4) replacing IgM based on the competitive nature of protein adsorption/exchange (5) adsorption of fibrinogen and washing away excess proteins (6) regeneration of the surface.

Once the SPR angle shift is stabilized, all the proteins on the surface including fibrinogen, IgM and other proteins are washed away by bleach. We use 0.9% sodium hypochlorite solution as the bleach that is effective to sanitize the sensing surface. It is relatively harmless to the surface of the biosensor because 0.0075% sodium hydroxide is used to delay the breakdown of sodium hypochlorite into sodium chloride and sodium chlorate. The regeneration enables multiple measurements of fibrinogen level in human serum on the same biosensor chip that can reduce irreproducibility and enhance controllability of multiple measurements. This regenerative biosensor potentially may be used to diagnose risk of cardiovascular disease.

2.2 Materials and Methods

Human serum and human IgM (Solution in 0.05 M Tris-HCl, 0.2 M sodium chloride, pH 8.0, containing 15 mM sodium azide) were purchased from Sigma-Aldrich. Fibrinogen was received as lyophilized powders from La Jolla Inc. and used without further purification. Bleach containing 6.0% sodium hypochlorite was diluted to 15% with DI water.

Initially, the biosensor surface was cleaned by bleach flowing through the microfluidic channel driven by an external syringe pump. Once the angle shift was stabilized, IgM was injected to pre-adsorb the biosensor surface at rate of 30 μL/min. The adsorption of IgM produces SPR angle shift. After the adsorption, phosphate-buffered

saline (PBS) was used to wash away any weakly bound IgM on the surface. This completes pre-adsorption process. We ensure the surface is saturated by IgM before we flow fibrinogen-spiked serum samples[7]. IgM has a molecular weight of approximately 900 kDa; thus it is one of the proteins with highest adsorption strength in serum. That means IgM is unlikely to be replaced by proteins with weaker adsorption strength in serum. It will be replaced by proteins with very strong adsorption strength such as fibrinogen.

a

b
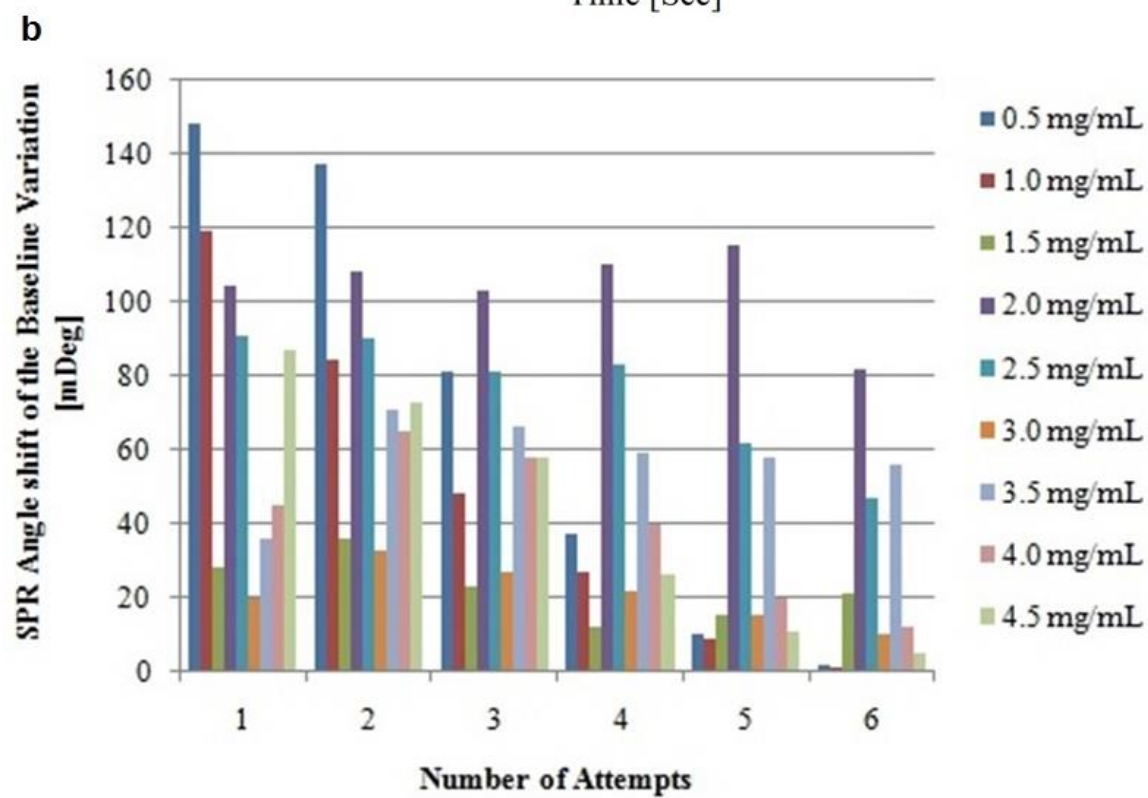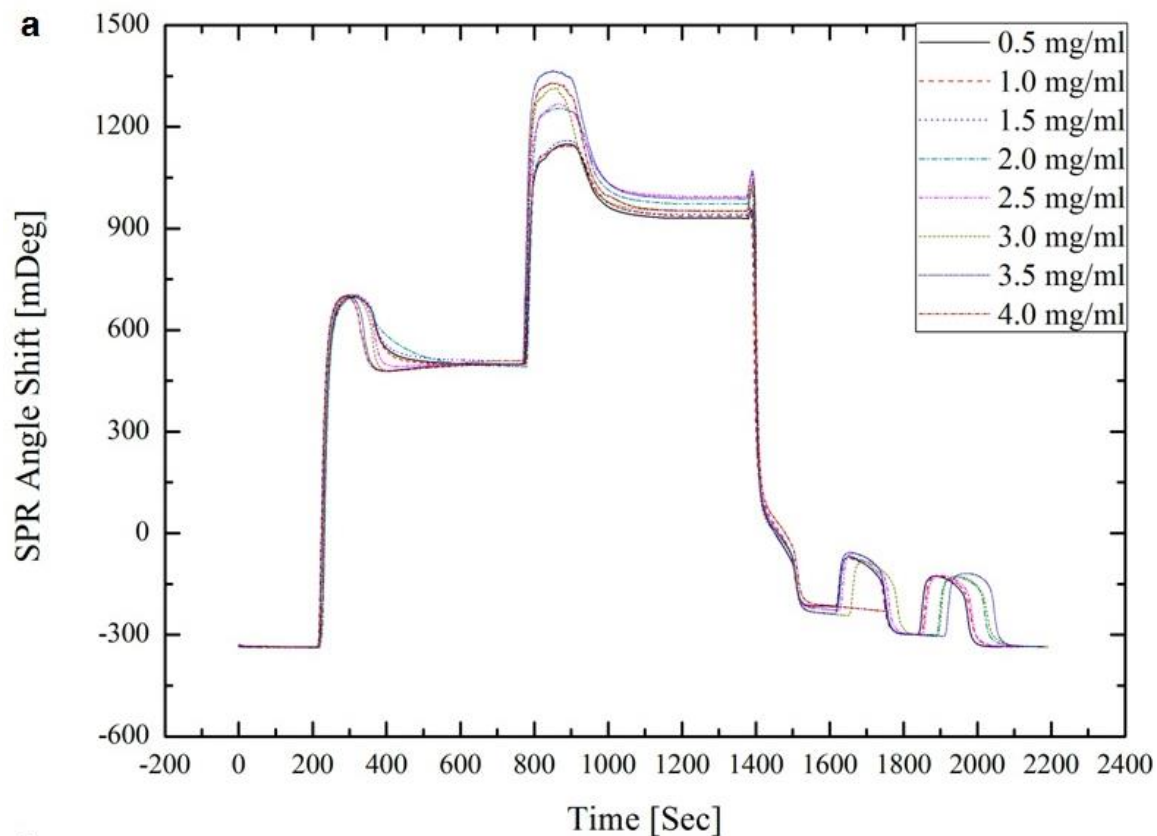
Figure 2.2 SPR angle shifts produced by fibrinogen samples with different concentrations. **a.** SPR sensorgrams of a series of fibrinogen-spiked serum samples ranging from 0.5 to 4.0 mg/mL. **b.** SPR angle shift of the baseline variation of fibrinogen-spiked serum ranging from 0.5 to 4.5 mg/mL.

Figure 2.2a illustrates SPR sensorgram of regeneration at different concentrations of fibrinogens on a chip, ranging from 0.5 to 4.0 mg/mL at 0.5 mg/mL intervals. Once the angle shift of IgM stabilized, the fibrinogen-spiked serum sample was injected at 30 µL/min and flowed through the surface that is pre-adsorbed by IgM. After washing away any weakly bound protein on the surface, we recorded the final angle shift from the baseline, which can be correlated to the concentration of fibrinogen. Finally, bleach was used to regenerate the biosensor chip at 50 µL/min three times to ensure removing all proteins on the surface till the baseline recovered.

In addition to the attempts of different concentrations on a chip, we also conducted sets of experiments regenerating the same concentrations of fibrinogen on a chip as well. Each concentration set of fibrinogen-spiked solutions was repeated six times and the SPR baseline variations as a function of the number of regeneration attempts are shown in Figure 2.2b. The regeneration solution cannot completely remove all the absorbed proteins on the surface. The data shows a general trend of decreasing the baseline variations as the number of attempts increased. After six attempts of regeneration, the baselines return nearly back to the original.
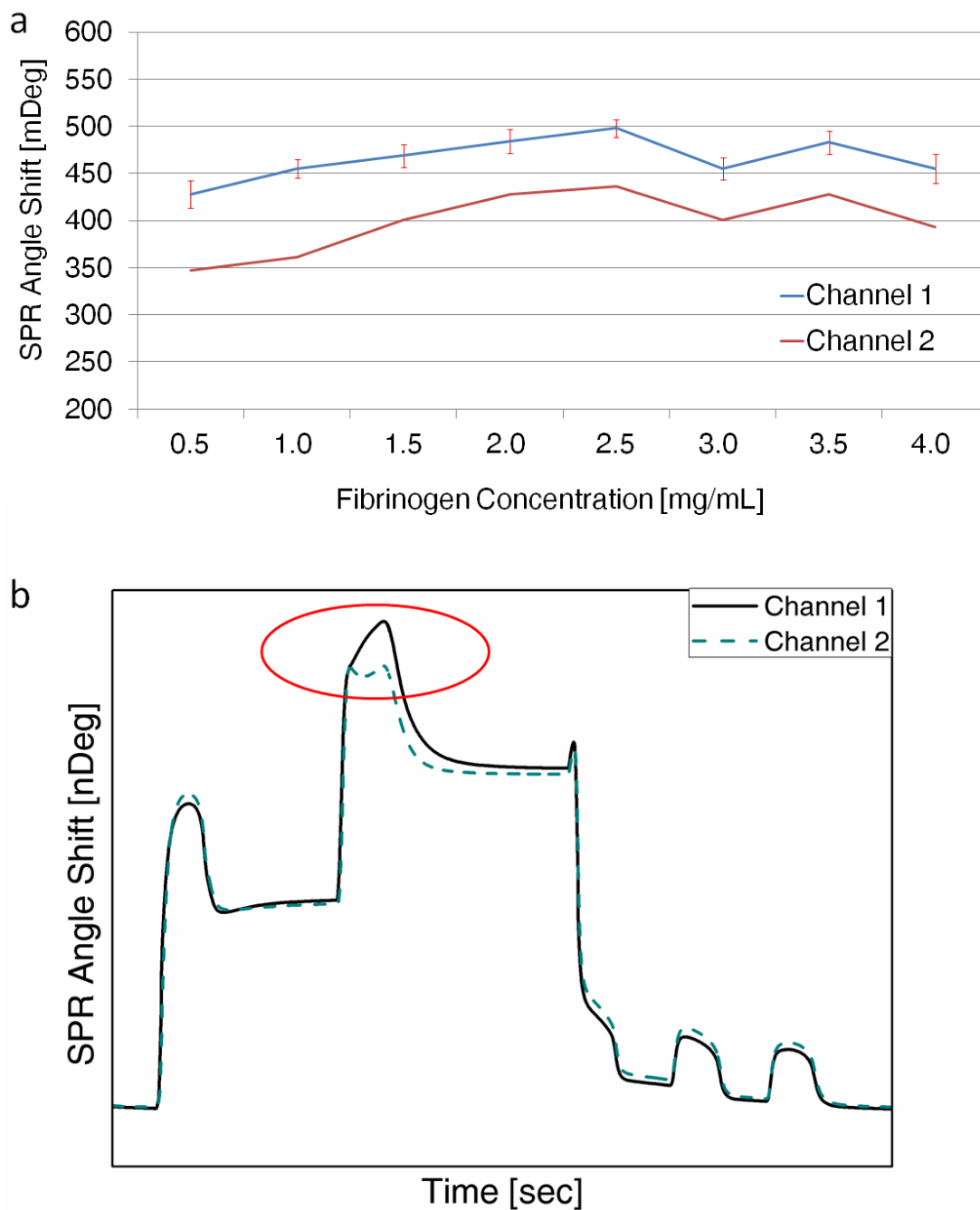
Figure 2.3 The deformation of SPR angle shifts caused by the coagulation of fibrinogen-spiked samples. **a.** SPR angle shifts as a function of fibrinogen concentration from 0.5 to 4.0 mg/mL. The plot was generated for 6 repeated trials at each concentration. SPR angle shifts of two channels were compared to examine the possibility of coagulation of fibrinogen-spiked samples **b.** Two real-time monitored SPR angle shift plots were compared to illustrate the deformation of channel 2.

Figure 2.3a plots a summary of the experiments in two channels showing SPR angle variations as a function of different concentrations of fibrinogen-spiked serum from 0.5 to 4.0 mg/mL.

2.3 Results and Discussion

In Figure 2.3a, we demonstrate that we can differentiate different concentrations of fibrinogen human serum samples from 0.5 to 2.5 mg/mL. Each data point represents the average measured angle shift over 6 repeated measurements for a particular concentration of fibrinogen. In order to scrutinize the possibility of coagulation of fibrinogen-spiked serum samples, we recorded SPR angle shifts of both channel 1 and 2.

Fibrinogen concentrations of less than 2.5 mg/mL exhibit a linear relationship to SPR angle shift, with a slope of 42 mDeg/(mg/mL). However, above a concentration of 2.5 mg/mL, the angle shift actually decreases and fluctuates. There are three hypothetical reasons for the discernible nonlinear phenomena that occur at concentrations greater than 2.5 mg/mL: i) saturation, ii) coagulation, and iii) decrease in sensitivity.

The first hypothesis that the sensor surface saturates for concentrations above 2.5 mg/mL seems unlikely to rationalize the observed nonlinear phenomena. If the surface was saturated, the SPR angle shifts observed for increasing concentrations above 2.5 mg/mL, should remain constant, rather than fluctuating. The SPR instrument includes two channels that are sequentially connected; fibrinogen-spiked samples flow through channel 1 and then through channel 2. If the sensing surface in channel 1 was saturated, the SPR angle shift of channel 2 for a fibrinogen concentration of 3.0 mg/mL should keep increasing until as high as the angle shift of channel 1, but instead follow a similar trend to that of channel 1. This

21

is because the slopes of the two curves (channels 1 and 2) are nearly identical (42 mDeg/(mg/mL) and 44 mDeg/(mg/mL) for channels 1 and 2, respectively), which confirms that both channels possess the same sensitivity.

Coagulation, the second hypothetical explanation for unforeseen phenomena observed at fibrinogen concentrations above 2.5 mg/mL, forms faster and more profusely if the concentration of fibrinogen is higher for a longer period[36]. As coagulation increases in the human serum, fewer proteins dissolve in the sample, leading to a lower fibrinogen concentration. This hypothesis is suggested by the measurement of the reduced angle shifts in channel 2 as compared to channel 1. As a result, there exist two factors determining the final concentration of fibrinogen: the initial concentration and coagulation level. Higher initial fibrinogen concentration results in a greater amount of coagulation, which may lead to a lower final concentration of fibrinogen. Consequently, a higher initial concentration may not necessarily produce a higher SPR angle shift. Further evidence to attribute coagulation to the unexpected nonlinear phenomena is the shape deformation observed during real-time SPR angle shift measurements, as encircled in Figure 2.3b. The maximum angle shifts in channel 2 are noticeably deformed as compared to the angle shifts measured in channel 1. Although it is difficult to entirely avert fibrinogen coagulation due to the clotting nature of fibrinogen, preventative measures may be taken to reduce coagulation; reducing sample preparation time and washing the micro-channels immediately after samples are processed through them. Without these anticipatory measures, the experimental data is likely to deviate and succumb to error and the microfluidic system in the SPR instrument will need to be disassembled to clean out the clot due to coagulation.

The third hypothetical reason is a reduction of sensitivity due to the damage on the surface of the biosensor chip caused by multiple regeneration cycles using bleach. In order to assess the decrease in sensitivity, we started the experiments with the fibrinogen concentration of 1.5 and 2.5 mg/mL separately. We increased the fibrinogen concentration by 0.5 mg/mL per regeneration cycle for the two sets of experiments. If the sensitivity of the biosensor chip had been reduced due to multiple bleach washing sequences and this reduced sensitivity was the cause for the angle shift to decrease above a fibrinogen concentration of 2.5 mg/mL, in these two experiments, the first regeneration cycles should not be affected significantly and the angle shift should keep increasing, because the bleach does not damage the biosensor surface seriously in the first regeneration cycles. Nevertheless, the angle shift observed at a concentration of 2.5 mg/mL was still the maximum angle shift measured for all concentration levels and the angle shift still fluctuated in the range of 2.5 to 4.5 mg/mL. For all of the aforementioned reasons, a possible reduction in sensitivity of the biosensor chip fails to substantiate the SPR angle shift decrease and fluctuations observed above concentrations of 2.5 mg/mL.

As a result, the first and third possibilities, saturation and possible sensitivity reduction, respectively, are unlikely to be attributable to the unexpected angle shift decrease and fluctuations seen at concentrations greater than 2.5 mg/mL. Instead, the second purported hypothesis, coagulation, remains the most probable grounds for the nonlinear phenomena.

CHAPTER 3

PROBING THYROGLOBULIN IN UNDILUTED HUMAN SERUM

3.1 Introduction

In this work, we aim to detect thyroglobulin (Tg, 660 kDa), a sensitive indicator of persistent or recurrent differentiated thyroid cancer (DTC) of follicular cell origin after total thyroidectomy[41, 42], in undiluted human serum.

Tg is produced by and used entirely within the thyroid gland. After total thyroidectomy, its normal concentration in serum is extremely low, less than 3 ng/mL when receiving thyroid hormone[41]. The current standards to measure Tg in serum are radioimmunoassay (RIA) and enzyme-linked immunesorbent assay (ELISA)[41]. Both are technically matured and commercialized. However, RIA involves complicated and time-consuming processes, including specific binding of antibody, labeling of gamma-radioactive isotopes, and separation of analytical labeled components from the mixture via precipitation and centrifugation. ELISA utilizes colorimetric signals to measure the antigen-antibody reaction instead of a radioactive method, which is more practical to supplant RIA[43]. These two techniques both suffer from non-specific interference in the process of specific binding between antigen and antibody[43, 44].

In order to circumvent the use of bio-receptors, we instead utilize the competitive adsorption of proteins, termed the Vroman effect. When lower-affinity proteins are adsorbed on the surface first, they can be displaced by higher-affinity proteins arriving at the surface at a later point in time. Moreover, only low-affinity proteins can be displaced by high-affinity proteins, typically possessing higher molecular weight, yet the reverse

sequence does not occur. Through SPR, the process of competitive protein adsorption may be monitored in real-time, and transduced into an SPR angle shift, as shown in Figure 3.1a&b.

The non-specific interference is a challenge to the Vroman effect based detection scheme as well. Only relying on the specific adsorption behavior is not sufficient to discriminate such minute concentrations of a target analyte (i.e., Tg in the range of <3 ng/mL) in human serum. In order to address the challenge, we combined the Vroman effect with a pattern recognition technique, a strategy based on the "chemical nose-tongue"[45-47], often used to detect multiple high-concentration target molecules in a complex mixture by discriminating specific fingerprints generated by a large array of biosensors. In the pattern recognition technique, an array of individual biosensor elements are used to provide sensing based on "differential" receptors. "Cross-responsive" interactions between biosensors in the array and the target proteins generate a unique composite pattern, which allows the recognition of the target proteins[48-51].

Selection of the sensing surfaces to generate input samples is critical as it affects the sensitivity and selectivity of a pattern recognition technique. 10 different sensing surfaces are designed to deliver large differences in adsorption affinity quantified by dissociation constant (K_D) and the change in Gibbs energy ($\Delta G°$). Among many statistical methods, Linear Discriminant Analysis (LDA), a robust pattern recognition technique, is adopted for this work[34]. Two kinds of results are produced to estimate the classification accuracy. The first is the original classification result that indicates how well the functions discriminate the given samples. The second is the cross-validation on the basis of the leave-

one-out option. These results can be used to estimate how well the functions should predict a new sample.

Table 3.1 Matrix of ten surface features for sensitivity characterization

		Pre-adsorbed proteins				
		Transferrin	Lysozyme	Albumin	IgM	IgG
Surfaces	Bare gold	SF 1	SF 2	SF 3	SF 4	SF 5
	COOH-SAM modified	SF 6	SF 7	SF 8	SF 9	SF 10

* SF: Surface Feature

a low-affinity proteins → high-affinity proteins

large $\Delta\theta$

SPR angle shift

Time
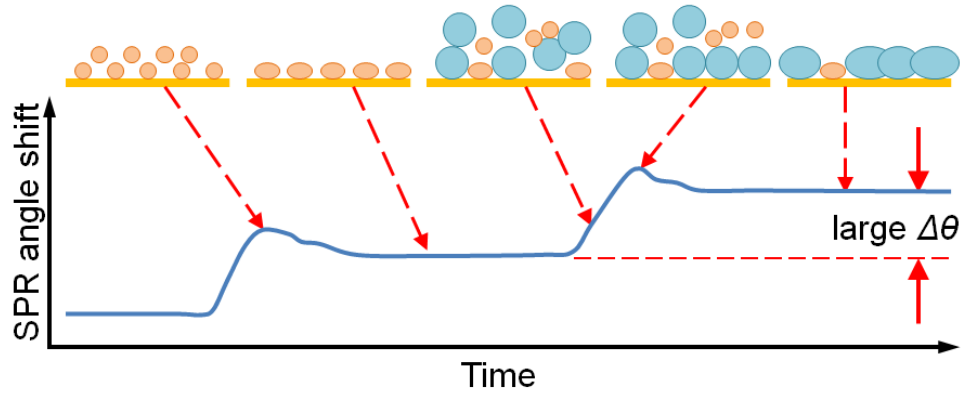
b high-affinity proteins → low-affinity proteins

$\Delta\theta \approx 0$

SPR angle shift

Time

c

SPR angle shift pattern

Known-affinity Proteins injection

Pre-adsorption
gold

Tg-spiked human serum

Competitive adsorption

Protein 1

Surface feature 1
COOH-SAM

Protein 2

Surface feature 2

Tg

Final SPR angle shift

Surface feature 1   Surface feature 2

SPR angle shift

Final SPR angle shift
baseline

Time
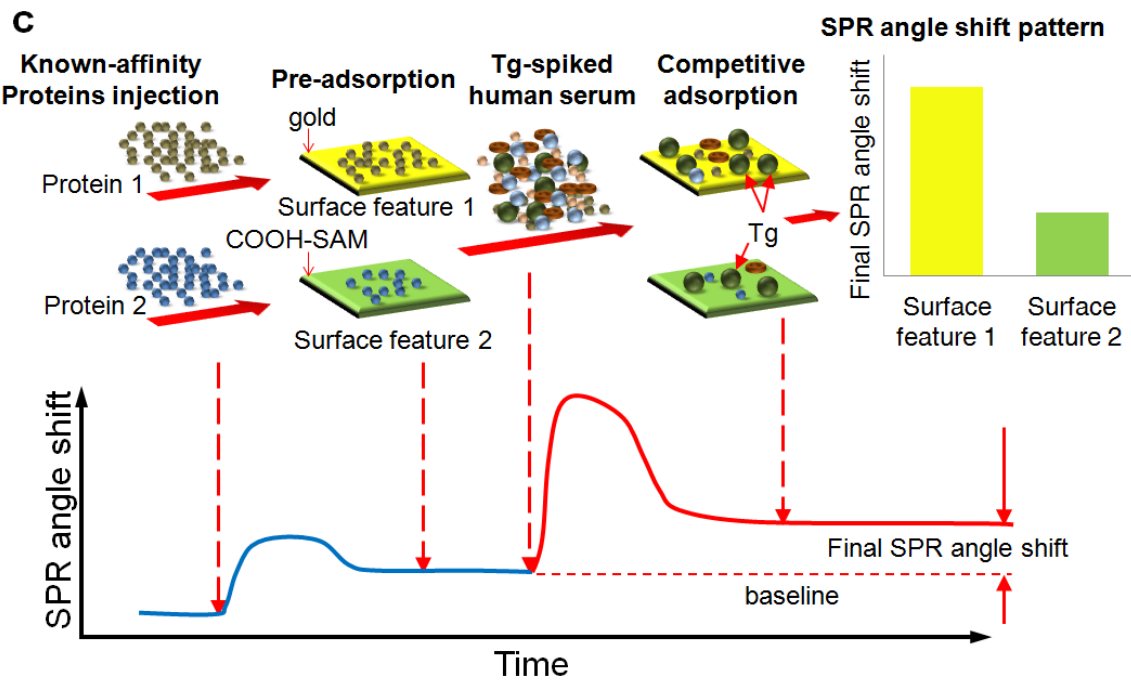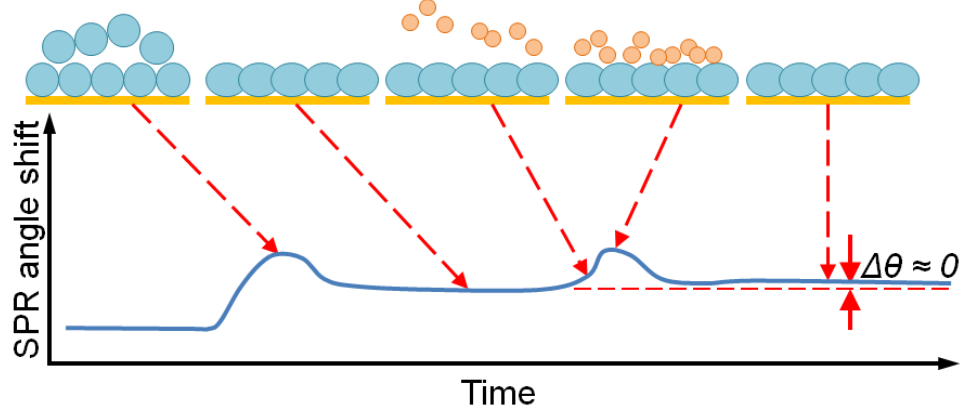
Figure 3.1 Illustration of the competitive adsorption of proteins (Vroman effect) and the schematics of SPR (Surface Plasmon Resonance) profile. **a.** Low-affinity proteins pre-adsorbed on a surface are displaced by high-affinity proteins arriving later, resulting in a large SPR angle shift, $\Delta\theta$. **b.** The reverse sequence does not lead to the displacement: high-affinity proteins pre-adsorbed on a surface are not displaced by subsequent low-affinity proteins. **c.** The SPR angle profile describing the competitive adsorption of proteins on two surface features (gold and COOH-SAM modified) generating a unique signature of Thyroglobulin (Tg) in human serum. The two surface features pre-adsorbed by known-affinity proteins generate distinctively different SPR angle shift patterns when they are exposed to samples containing Tg.

The bare gold or COOH-SAM modified sensing surface is mounted above the SPR, which is then coupled with the flow cell. After thorough calibration, each one of the five known-affinity protein (IgM, IgG, Transferrin, Albumin, and Lysozyme) samples is injected to be pre-adsorbed on a bare gold surface. Besides the bare gold surface, these five protein samples are also separately pre-adsorbed on the COOH-SAM modified surface. These five different proteins and two different surfaces provide ten types of surface features (Table 3.1) for Tg detection, establishing the array that generates a pattern. When pre-adsorption is completed, Phosphate Buffered Saline (PBS) rinses the surface to sweep excess weakly bound proteins so that a stable baseline is established for the subsequent step, Tg detection. Tg-spiked (100, 10, and 2 ng/mL) serum samples flow across the pre-adsorbed surfaces. The SPR angle shift increases simultaneously as some pre-adsorbed proteins are replaced by Tg via the competitive adsorption behavior of proteins. After rinsing and sweeping with PBS, the SPR angle shift reaches steady state. Subtracting the baseline from this angle shift, a final angle shift caused by Tg-spiked samples is obtained (Figure 3.1c). Individual surface features generate their own angle shifts. Every sample is repeated 6 times on every surface feature and ten average values of SPR angle shifts from ten surface features are obtained to form a distinguishing pattern for each sample. Different

28

patterns are compared and analyzed to discriminate the Tg-spiked samples as a function of Tg concentrations in undiluted serum.

Proteins are differently adsorbed on the surfaces with different characteristics based upon their thermodynamic energy preferences, and naturally behave to minimize the overall system energy[28]. Their reactions can be interpreted as the natural outcome to achieve the equilibrium point. Therefore, the change in Gibbs energy caused by protein adsorption on a surface reflects the chemical potential and reaction process in the system[52, 53].

The change in Gibbs energy for the reversible part of the adsorption process can be expressed as:

$$\Delta G = \Delta G^o + RT\left([AB]/\left([A][B]\right)\right) \qquad 3.1$$

and at equilibrium:

$$\Delta G^o = -RT\ln\left([AB]/\left([A][B]\right)\right) = -RT\ln\left(\Delta\theta/\left(C\left(\Delta\theta_{max} - \Delta\theta\right)\right)\right) = RT\ln\left(K_D\right) \qquad 3.2$$

where ΔG and $\Delta G°$ represent the changes in adsorption free energy and in standard state adsorption free energy, respectively; R is the ideal gas constant (1.985 cal/K•mol); and T is the absolute temperature (298K). $[A]$ is the molar concentration of the protein in solution; $[B]$ and $[AB]$ are the mole fraction of surface sites occupied by a surface and adsorbed protein, respectively. $\Delta\theta$ is the SPR angle shift; $\Delta\theta_{max}$ is the SPR angle shift at the saturation; C is the protein concentration; K_D is the dissociation constant[28, 53].
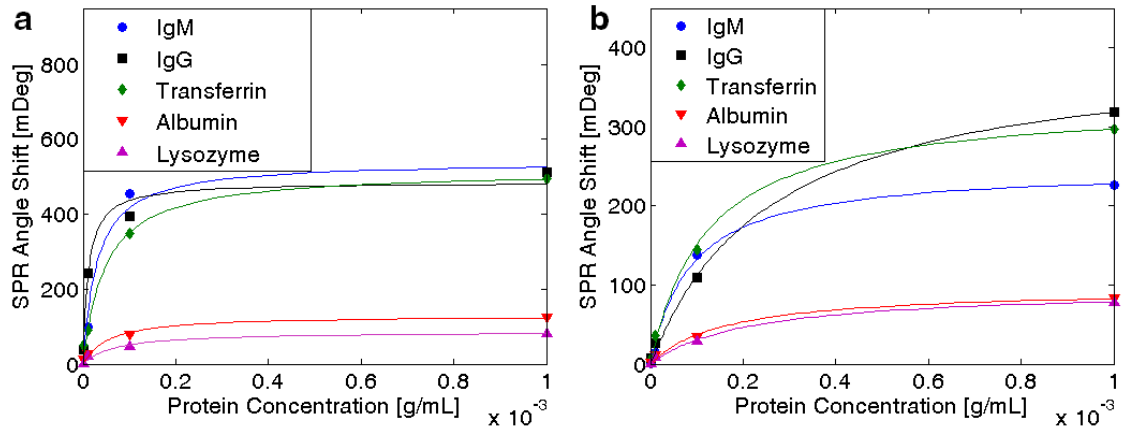
Figure 3.2 SPR angle shift as a function of protein concentrations on **a.** bare gold surface and **b**. COOH-SAM modified gold surface. Five proteins, IgM, IgG, Transferrin, Albumin, and Lysozyme, are characterized for their adsorption on the two surfaces at 0.001, 0.01, 0.1, and 1 mg/mL in PBS.

Through Eq. (2), a Langmuir-like feature, as shown in Figure 3.2, can be described by[53]:

$$\Delta\theta = \Delta\theta_{\max} C/(K_D + C) \qquad\qquad 3.3$$

Noticeably, as SPR signal changes are probably not taken under truly equilibrium states, the extracted dissociation constants (K_D) are apparent and useful only for the purpose of comparing results obtained under similar experimental conditions[54].

Table 3.2 Ten surfaces described by protein characteristics, equilibrium dissociation constants (K_D) and the changes in Gibbs energy (ΔG^o)

Protein characteristics			Surface	$\Delta\theta_{max}$ (mDeg)	K_D (10^{-5} M) ±s.d.	ΔG^o (Kcal/mol) ±s.d.
Protein	Molecular weight (kDa)	Isoelectric point				
IgM	970	5.7	bare gold	501	1.0±0.1	-6.8±0.04
			COOH-SAM	222	6.0±0.3	-5.7±0.03
IgG	150	7.6	bare gold	517	3.1±0.1	-6.1±0.02
			COOH-SAM	295	17±1.6	-5.1±0.06
Transferrin	80	5.6	bare gold	504	4.5±0.2	-5.9±0.02
			COOH-SAM	295	10.3±0.1	-5.4±0.01
Albumin	76	5.2	bare gold	117	5.0±0.7	-5.9±0.09
			COOH-SAM	80	12.9±0.6	-5.3±0.03
Lysozyme	14.7	9.2	bare gold	87	8.8±0.5	-5.5±0.04
			COOH-SAM	80	17.4±0.4	-5.1±0.01

Successful pattern recognition relies upon the distinctive patterns that are facilitated by the discrepancies of protein behaviors on each surface feature in the biosensor array. In other words, a protein pre-adsorption on a surface should generate a surface feature possessing unique sensing characteristics, so that the displacements by Tg on the surface feature results in a unique SPR angle shift. The final organization of the surface adsorbing proteins depends on many factors: the chemical and physical structure of the proteins, the hydrophobicity or hydrophilicity of the surface, the kinetics of proteins' movement and spreading, the thermodynamics of the interactions between these system components, etc[52-54]. Table 3.2 lists maximum SPR angle shift (at saturation), $\Delta\theta_{max}$, equilibrium dissociation constant, K_D, and Gibbs energy change, $\Delta G°$, measured on ten different surface features

between five different proteins, IgM, IgG, Transferrin, Albumin, Lysozyme and two surfaces, bare gold and COOH-SAM modified gold surface.

3.2 Materials and Methods

Five different proteins are utilized to be pre-adsorbed on the surfaces of gold chips. Four of them are received as lyophilized powders from Sigma-Aldrich and used without further purification: IgG (150 kDa), Transferrin (80 kDa), Albumin (67 kDa), Lysozyme (14.7 kDa). IgM (900 kDa) is received as buffered aqueous solution (~95% by HPLC, 0.9 mg/mL). Thyroglobulin (Tg, 660 kDa) is purchased from Calbiochem in the form of Lyophilized powder and used without further purification. Lysozyme, Transferrin, Albumin and IgG powders are prepared in Phosphate Buffered Saline (PBS) with concentrations of 1 mg/mL each. Tg powders are dissolved in human serum at three different concentrations: 100 ng/mL, 10 ng/mL and 2 ng/mL. The concentrations gradually decrease to attempt the lowest limitation of this biosensor. 11-mercaptoundecanoic acid (95%) from Sigma-Aldrich is used to form COOH-terminated SAM (self-assembled monolayer).

With k classes, LDA produces $k-1$ discriminant functions that produce the greatest discriminations between these k classes. These functions are the eigenvalues of the ration of between-class covariance and in-class covariance. This ration is used to highlight the discrepancies between classes. The eigenvectors of the ratio are the best directions to discriminate these classes. The largest eigenvalue represents that the corresponding eigenvector is the best direction to separate the classes. If there are more than three functions produced, three of them, which contain as much of the distinguishing signals of

the original data set as possible and are uncorrelated to each other, are picked up to build a plot in three dimensions. Particularly, in this work, a kind of sample represents a class. The data set contains SPR angle shift patterns representing different samples, generated from ten types of surface features that include five different proteins pre-adsorbed on bare gold surface and COOH-SAM modified gold surface. In the plot, every data point, or training case, represents a replication generated from ten different surface features. The data points (six points produced by six replications) representing the same sample are separated from others, if they can be successfully recognized.

To modify the bare gold chips with COOH-terminated SAM, the gold chips fabricated above are immersed in an ethanol (Proof 200) solution of alkane-thiols (1 mM) for 24 hours. Before use, they are rinsed with ethanol and dried by a N_2 stream. Compared with hydrophobic bare gold surfaces, COOH-SAM modified chips are hydrophilic, which leads to different interaction with proteins[34].

3.3 Results and Discussion

3.3.1 Sensitivity of SPR Biosensor

The normal concentration of Tg in human serum is 3 ng/mL for a patient after treatment for DTC. In order to characterize the sensitivity of biosensor for diagnosis, three different Tg-spiked samples, 100 ng/mL, 10 ng/mL, and 2 ng/mL, are attempted, and undiluted human serum is used as the control.
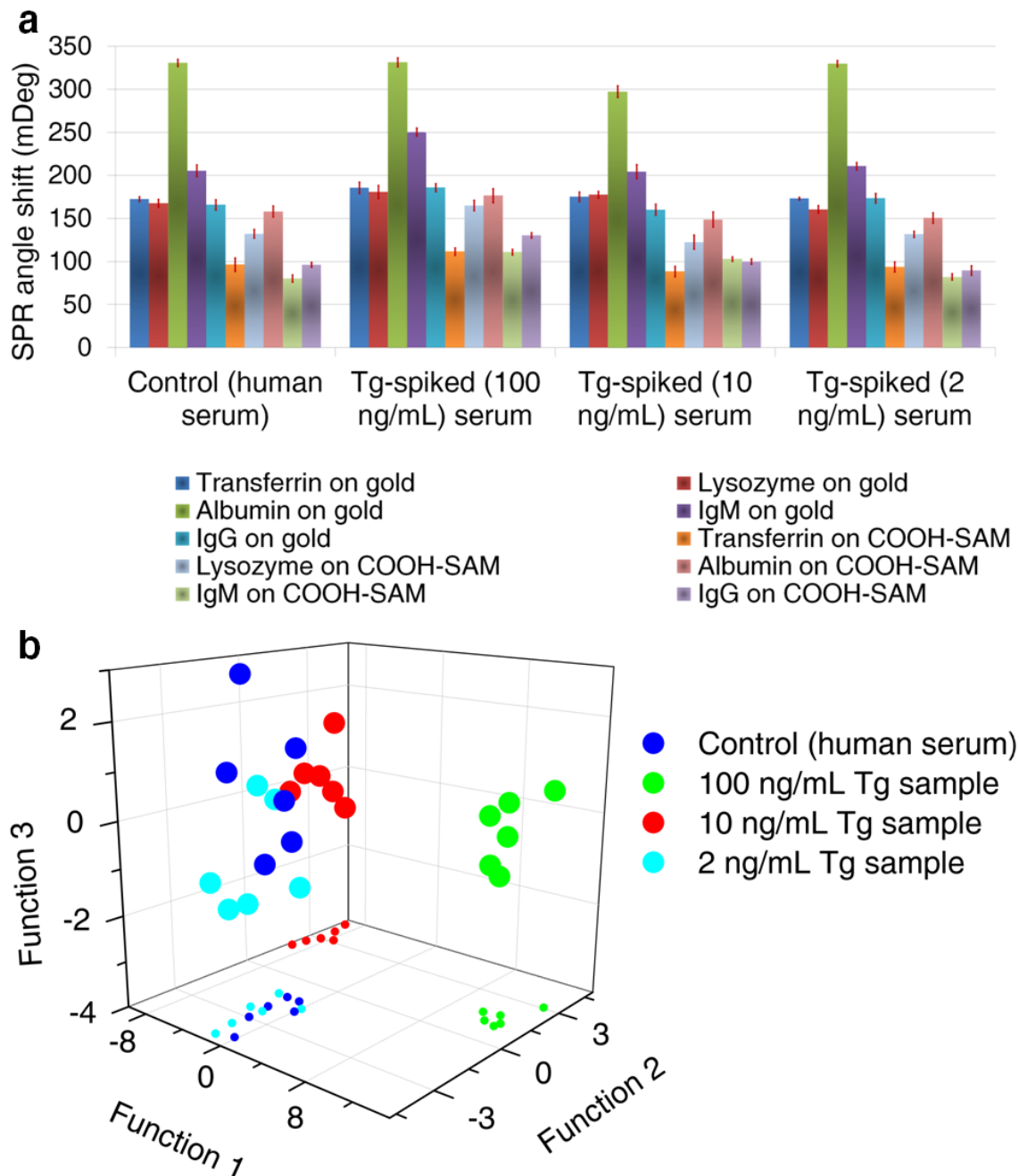
Figure 3.3 Sensitivity characterization **a.** SPR angle shifts of 100 ng/mL, 10 ng/mL, 2 ng/mL Tg-spiked samples and the control (undiluted human serum) from ten surface features (6 replications for each sample) **b.** Four groups of six data points, corresponding to 100 ng/mL, 10 ng/mL, 2 ng/mL Tg-spiked samples and the control, on three most significant discriminant functions obtained from LDA (Linear Discriminant Analysis). Each data point represents a replication generated from ten surface features. Four groups of six data points are projected on the plane of two most significant discriminant functions.

Finite amount of overlap exists between the control (blue-colored dots) and 2 ng/mL Tg-spiked sample (cyan-colored dots), showing the difficulty of discrimination due to the similarity of these two samples, which can be partially discriminated by another function (z-axis).

The measurements for all cases are repeated 6 times to demonstrate the stability and reliability. Ten different surface features produced $6 \times 10 = 60$ SPR angle shifts that together form a group representing a single sample. As such, the four samples (100, 10, 2 mg/mL Tg-spiked samples and the control) are represented by four groups of SPR angle shifts. All the SPR angle shifts are listed in Table 3.3&3.4. In Figure 3.3a, ten average values with error bars (standard deviation) taken from the ten different surface features and measured over six repetitions are shown to form a pattern. Depending on the specific response on one kind of surface feature, the difference between the sample and the control are usually too minute to be discriminated. These SPR angle shift patterns are further analyzed by LDA to be discriminated and formally classified into different groups.

Table 3.3 Matrix of five samples

Sample 1	Sample 2	Sample 3	Sample 3	Sample 4
Human serum	100 ng/mL Tg-spiked human serum	10 ng/mL Tg-spiked human serum	2 ng/mL Tg-spiked human serum	100 ng/mL IgM-spiked human serum

Table 3.4 Matrix of SPR response signals of five samples

	SPR angle shift [mDeg]									
	SF 1	SF 2	SF 3	SF 4	SF 5	SF 6	SF 7	SF 8	SF 9	SF 10
	169	167	335	220	178	77	138	145	85	97
	170	175	336	198	163	81	141	142	88	94
Sample 1	184	175	324	191	170	120	135	173	84	99
	173	164	317	221	154	100	134	159	86	89
	170	152	337	193	180	98	133	170	69	105
	170	174	336	210	151	103	113	160	70	93
	190	190	323	254	176	116	175	183	116	138
	184	198	330	248	175	105	171	195	110	126
Sample 2	203	171	318	248	192	103	178	180	100	136
	189	195	338	235	186	104	162	188	111	122
	186	167	334	261	188	124	160	158	110	127
	163	164	346	257	199	118	145	156	119	134
	187	173	281	230	173	93	105	170	106	103
	182	176	314	220	153	88	100	164	105	99
Sample 3	179	176	290	190	172	94	140	143	100	102
	157	187	287	198	150	93	134	150	110	109
	180	167	303	196	144	98	130	120	96	91
	168	187	310	193	170	65	127	146	101	96
	178	150	326	200	174	104	137	166	80	90
	175	174	328	224	170	96	126	161	74	70
Sample 4	170	166	334	215	182	100	141	135	94	91
	170	158	331	210	190	80	134	138	84	87
	173	160	320	213	165	105	122	155	85	98
	173	156	341	203	160	78	130	149	76	102
	171	211	311		200	102	155	179		143
	168	194	314		220	104	148	180		140
Sample 5	165	178	335		193	102	158	170		139
	191	186	315		213	92	153	216		142
	181	186	320		200	115	155	197		120
	175	175	310		202	122	148	196		144

* SF: Surface Feature

After LDA, three discriminant functions are generated (90.0%, 9.6% and 0.4%) to represent the linear combinations of the ten-dimensional data set including four samples × ten surface features × six replications. Based on the three functions, a three dimensional plot is built in Figure 3.3b, in which 24 training cases (4 samples × 6 replications) are

classified into four groups representing four samples, respectively. In Table 3.5, the

original classification of 91.7% indicates how well the functions discriminate these four

given samples, while the cross-validations of 66.7% is used to estimate how well the

functions derived from all 24 cases should predict a new sample.

Table 3.5 Classification results[b,c] for sensitivity characterization

Categories			Predicted Group Membership				Total
			Control (serum)	Tg (100 ng/mL)	Tg (10 ng/mL)	Tg (2 ng/mL)	
Original	Count	Control (serum)	5	0	0	1	6
		Tg (100 ng/mL)	0	6	0	0	6
		Tg (10 ng/mL)	0	0	6	0	6
		Tg (2 ng/mL)	1	0	0	5	6
	%	Control (serum)	83.3	.0	.0	16.7	100.0
		Tg (100 ng/mL)	.0	100.0	.0	.0	100.0
		Tg (10 ng/mL)	.0	.0	100.0	.0	100.0
		Tg (2 ng/mL)	16.7	.0	.0	83.3	100.0
Cross-validated[a]	Count	Control (serum)	2	0	0	4	6
		Tg (100 ng/mL)	0	6	0	0	6
		Tg (10 ng/mL)	0	0	6	0	6
		Tg (2 ng/mL)	4	0	0	2	6
	%	Control (serum)	33.3	.0	.0	66.7	100.0
		Tg (100 ng/mL)	.0	100.0	.0	.0	100.0
		Tg (10 ng/mL)	.0	.0	100.0	.0	100.0
		Tg (2 ng/mL)	66.7	.0	.0	33.3	100.0

a. Cross validation is done only for those cases in the analysis. In cross validation, each case is classified by the functions derived from all cases other than that case.
b. 91.7% of original grouped cases correctly classified.
c. 66.7% of cross-validated grouped cases correctly classified.

We further analyze the separate discriminating accuracies for the three Tg samples

(Table 3.6-3.8). 100, 10, and 2 ng/mL Tg-spiked samples that are discriminated from the

control show the original classification of 100 %, 100 %, and 100 %, and the cross-

validation of 83.3 %, 53.3 %, and 41.7%, respectively. In other words, for an unknown

sample, a higher concentration evidently provides a higher possibility to discriminate Tg samples from the control. In Figure 3.3b, 100 ng/mL and 10 ng/mL Tg-spiked serum samples are shown farther away from the control, but the 2ng/mL Tg-spiked serum sample has a finite overlap with the control, which highlights the difficulty of discrimination. The reason is apparent in the case where more differences between higher concentration Tg samples and the control result in more distinctively different patterns that are easier for LDA to discriminate.

Table 3.6 Classification results of 100 ng/mL Tg-spiked serum[b,c]

		categories	Predicted Group Membership 1	2	Total
Original	Count	1	6	0	6
		2	0	6	6
	%	1	100.0	.0	100.0
		2	.0	100.0	100.0
Cross-validated[a]	Count	1	4	2	6
		2	0	6	6
	%	1	66.7	33.3	100.0
		2	.0	100.0	100.0

[a]. Cross validation is done only for those cases in the analysis. In cross validation, each case is classified by the functions derived from all cases other than that case.
[b]. 100.0% of original grouped cases correctly classified.
[c]. 83.3% of cross-validated grouped cases correctly classified.

Table 3.7 Classification results of 10 ng/mL Tg-spiked serum[b,c]

		categories	Predicted Group Membership 1	2	Total
Original	Count	1	6	0	6
		2	0	6	6
	%	1	100.0	.0	100.0
		2	.0	100.0	100.0
Cross-validated[a]	Count	1	1	5	6
		2	0	6	6
	%	1	16.7	83.3	100.0
		2	.0	100.0	100.0

[a]. Cross validation is done only for those cases in the analysis. In cross validation, each case is classified by the functions derived from all cases other than that case.

[b]. 100.0% of original grouped cases correctly classified.

[c]. 58.3% of cross-validated grouped cases correctly classified.

Table 3.8 Classification results of 2 ng/mL Tg-spiked serum[b,c]

		categories	Predicted Group Membership 1	2	Total
Original	Count	1	6	0	6
		2	0	6	6
	%	1	100.0	.0	100.0
		2	.0	100.0	100.0
Cross-validated[a]	Count	1	2	4	6
		2	3	3	6
	%	1	33.3	66.7	100.0
		2	50.0	50.0	100.0

[a]. Cross validation is done only for those cases in the analysis. In cross validation, each case is classified by the functions derived from all cases other than that case.

[b]. 100.0% of original grouped cases correctly classified.

[c]. 41.7% of cross-validated grouped cases correctly classified.

All the points, mapped on an x-y plane, are composed of two most significant

functions. This demonstrates that these four samples can be discriminated on an x-y plane

(or two functions). Only the discrimination between the 2 ng/mL Tg-spiked sample and the control needs the assistance of the third function.

3.3.2 Selectivity of SPR Biosensor

A set of experiments for selectivity of SPR biosensor are designed and executed. IgM is chosen to demonstrate the selectivity characterization as the affinity strength of IgM (K_D, 1.0×10^{-5} M, and ΔG^o, -6.8 Kcal/mol) is similar to that of Tg (K_D, 0.7×10^{-5} M, and ΔG^o, -7.0 Kcal/mol). Eight surface features produce the patterns for the 100 ng/mL IgM-spiked serum sample, as shown in Figure 3.4a. The corresponding SPR angle shifts are listed in Table 3.3&3.4. LDA is then performed to analyze these samples. Four functions are generated (84.6%, 11.9%, 3.1% and 0.4%) and the three most significant functions are used to build the three dimensional plot in Figure 3.4b. The plot shows that the IgM-spiked serum is clearly separated from other samples, except for a little overlap with the 100 ng/mL Tg-spiked serum. The original classification result and the cross-validation result are 90.0% and 63.3%, respectively, as listed in Table 3.9.
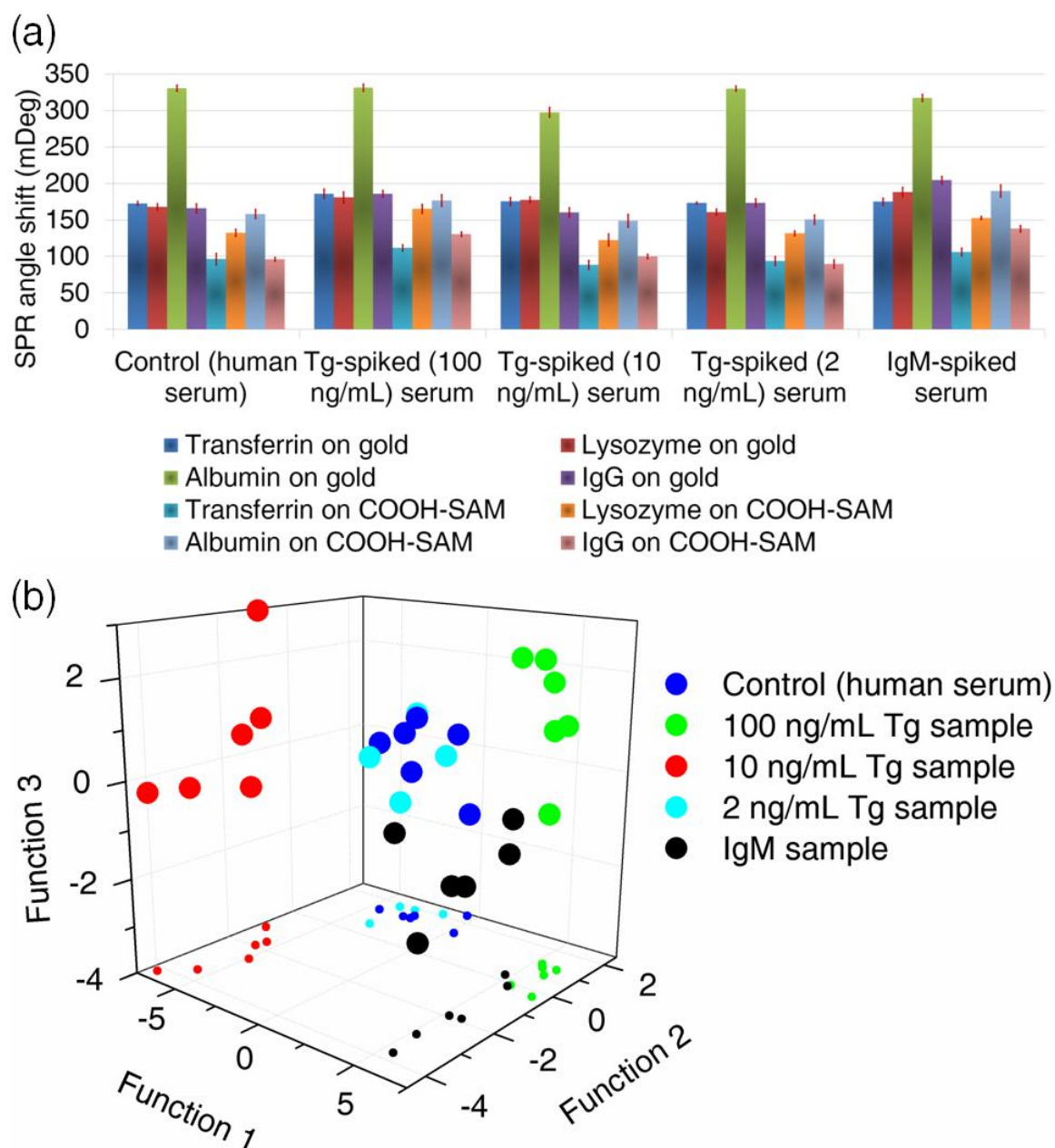
Figure 3.4 Selectivity characterization **a.** SPR angle shifts of 100 ng/mL, 10 ng/mL, 2 ng/mL Tg-spiked, 100 ng/mL IgM-spiked human serum samples and the control (undiluted human serum) from eight surface features (6 replications for each sample). **b.** Five groups of six data points, corresponding to 100 ng/mL, 10 ng/mL, 2 ng/mL Tg-spiked, 100 ng/mL IgM-spiked human serum samples and the control (undiluted human serum), on three most significant discriminant functions obtained from LDA. Each data point represents a replication generated from eight surface features. Five groups of six data points are projected on the plane of two most significant discriminant functions. Finite amount of overlap exists between 100 ng/mL Tg-spiked and 100 ng/mL IgM-spiked samples.

Notably, the control and 2 ng/mL Tg-spiked sample overlap more than Figure 3.3b as eight surface features provide weaker discriminating power than ten surface features do.

Table 3.9 Classification results[b,c] for selectivity characterization

	Categories		Predicted Group Membership					Total
			Control (serum)	Tg (100 ng/mL)	Tg (10 ng/mL)	Tg (2 ng/mL)	IgM (100 ng/mL)	
Original	Count	Control (serum)	4	0	0	2	0	6
		Tg (100 ng/mL)	0	6	0	0	0	6
		Tg (10 ng/mL)	0	0	6	0	0	6
		Tg (2 ng/mL)	1	0	0	5	0	6
		IgM (100 ng/mL)	0	0	0	0	6	6
	%	Control (serum)	66.7	.0	.0	33.3	.0	100.0
		Tg (100 ng/mL)	.0	100.0	.0	.0	.0	100.0
		Tg (10 ng/mL)	.0	.0	100.0	.0	.0	100.0
		Tg (2 ng/mL)	16.7	.0	.0	83.3	.0	100.0
		IgM (100 ng/mL)	.0	.0	.0	.0	100.0	100.0
Cross-validated[a]	Count	Control (serum)	2	0	0	4	0	6
		Tg (100 ng/mL)	0	5	0	0	1	6
		Tg (10 ng/mL)	0	0	6	0	0	6
		Tg (2 ng/mL)	4	0	0	2	0	6
		IgM (100 ng/mL)	0	2	0	0	4	6
	%	Control (serum)	33.3	.0	.0	66.7	.0	100.0
		Tg (100 ng/mL)	.0	83.3	.0	.0	16.7	100.0
		Tg (10 ng/mL)	.0	.0	100.0	.0	.0	100.0
		Tg (2 ng/mL)	66.7	.0	.0	33.3	.0	100.0
		IgM (100 ng/mL)	.0	33.3	.0	.0	66.7	100.0

a. Cross validation is done only for those cases in the analysis. In cross validation, each case is classified by the functions derived from all cases other than that case.
b. 90.0% of original grouped cases correctly classified.
c. 63.3% of cross-validated grouped cases correctly classified.

CHAPTER 4

DETECTION OF COPPER IONS IN DRINKING WATER

4.1 Introduction

Heavy metal ions refer to metallic elements, having a relative high density, such as iron, cobalt, copper, manganese, molybdenum, zinc, mercury, plutonium, and lead. Heavy metals are dangerous because they tend to bioaccumulate. Among them, copper ions are considered to be one of the critical heavy metal ions contained in drinking water as they are common contaminants produced by corrosion of household plumbing systems and erosion of natural deposits, and may induce gastrointestinal distress, even liver or kidney damage[55].

A number of techniques have been developed over the years for heavy metal ion analysis, including atomic absorption spectrometry[56], inductively coupled plasma mass spectrometry[57], anodic stripping voltammetry (ASV)[58, 59], X-ray fluorescence spectrometry[60], and microprobes[61]. For instance, ASV is a powerful established technology for detection of metal ions and other electrochemically active substances[62, 63]. However, ASV has several limitations, including the need of the use of supporting electrolyte, the use of mercury electrode, high background current challenging to detect small stripping current associated with oxidation of analytes, inability of detecting non-redox-active species, and formation of intermetallic compounds to disturb individual stripping peaks[64].

To design highly selective metal ion sensors, several innovative recognizing elements based on organic chelators[65], organic polymers[66], proteins[22], cells[67], DNA/RNA and peptides[58, 68-71] have been reported. However, most of these approaches are perhaps

challenged by the design and synthesis of sensors capable of specific and strong binding of the target metal ions but not other competing metal ions[72]. Besides, peptide biosensors are limited by the fact that many toxic metal ions do not have specific probes[53, 64]. DNA/RNA biosensors must be used under rigorous condition of measurement which must allow survival of the cell (narrow pH and temperature ranges, lack of other toxic compounds, etc.)[73]. Metal-binding proteins are synthesized by many cell types in response to the presence of specific metals and play important roles in metal homeostasis and detoxification mechanisms[23]. However, many technical challenges exist including complex overexpression and purification of proteins and labor-intensive, time-consuming processes[24, 25]. Therefore, a rapid, less-complex and inexpensive method that permits real-time detection of metal ions has been demanded for a variety of applications. In addition, due to the danger that the heavy metal ions pose to operators, minimal sample handling is desirable.

In this work, we report a unique sensing method of copper ions by combining Surface Plasmon Resonance (SPR), a surface-sensitive optical instrument, with competitive adsorption of proteins, termed the Vroman effect. SPR sensitively responds to minute change of refractive index at the vicinity of a sensing surface that may be produced by the conformation change of proteins, induced by copper ions. When albumins are engineered as the receptor of copper ions on the sensing surface, their conformation change is caused by disruption of ionic interactions (salt bridge) or disulfide bonds by copper ions[25, 74]. Consequently, these denatured albumins possess weaker affinity than native ones[11, 75]. By comparing the affinity of denatured albumins with that of native albumins it may be possible to distinguish one from the other. However, such direct comparison

44

method suffers from fluctuation of measurement. Here we propose a unique method to obviate the measurement accuracy challenge by adopting the competitive adsorption between them. The weaker denatured albumins pre-adsorbed on sensing surface can be replaced by native ones possessing stronger affinity. This competitive adsorption process may be real-time monitored by SPR, as shown in Figure 4.1a.
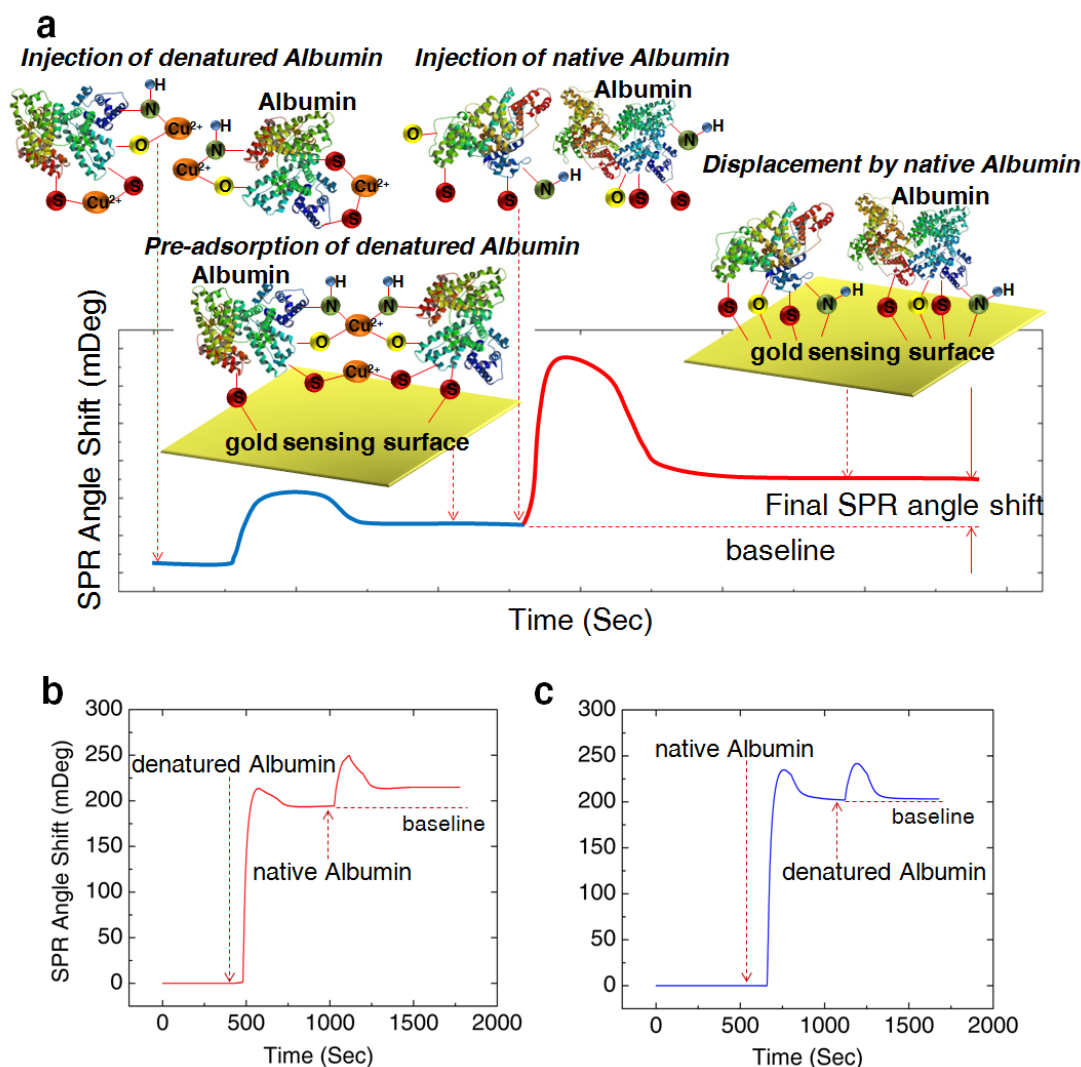
Figure 4.1 The SPR angle profile describes the competitive adsorption of albumins. **a.** Albumins are denatured by Cu^{2+}, through the disruption of ionic interactions and disulfide bonds. Due to the weaker affinity, the pre-adsorbed denatured albumins are displaced by native albumins. Consequently, the conformation change adjacent to the gold sensing surface generates the change of SPR angle shift. **b.** Consistent with a, the denatured

proteins are replaced by native ones, which generates the increase of SPR angle shift. **c.** However, the reverse sequence does not occur, and change of SPR angle shift is negligible.

We engineer the affinity of native albumins by introducing copper ions to disturb bonds of the albumins. Albumins are denatured by copper ions mainly due to the disruption of tertiary structure, in which copper ions disrupt ionic interactions (salt bridge) held together by ionic charges and disulfide bonds due to heavy metal ions' higher affinity and attraction for sulfur[11, 25, 74, 75]. The affinity of proteins to adsorb on a gold surface is believed to rely on, except for hydrophobic effect, the bonds of Au-COO, Au-N and Au-S[76-78]. Among these bonds, Au-COO and Au-N may be disrupted due to the disruption of ionic interactions (salt bridge), and Au-S may be disrupted due to the disruption of disulfide bonds. Therefore, the affinity of albumins adsorbed on the gold surface may be compromised. The discrepancy of protein affinity may be compared through the competitive adsorption. In this competitive process, weaker denatured albumins pre-adsorbing on the sensing surface should be replaced by native ones. This hypothesis is experimentally demonstrated through a sequence of SPR biosensing, as shown in Figure 4.1 b&c. Accordingly, the larger SPR angle shift represents the larger change of albumins' affinity caused by more disruption of conformation. The outcome is a rapid, less-complex, and inexpensive biosensor to be able to detect copper ions in drinking water.

4.2 Materials and Methods

Cu^{2+} (as CuCl2 $2H_2O$) are received as powder from Sigma-Aldrich. Albumin (67 kDa) is received as lyophilized powders from Sigma-Aldrich, and used without further purification. Albumin is prepared in Phosphate Buffered Saline (PBS) solution with

concentrations of 2 mg/mL. According to National Primary Drinking Water Regulations published by United States Environment Protection Agency (EPA), the Maximum Contaminant Level (MCL) of copper ions in drinking water is 1.3 mg/L. Thus, $CuCl_2 \cdot 2H_2O$ are prepared at six different Cu^{2+} concentrations: 2.5, 1.3, 1.0, 0.5, 0.3, and 0.1 mg/L.

2 mg/mL albumin samples are spiked by Cu^{2+}, Fe^{3+}, Mn^{2+}, Pb^{2+} and Hg^{2+}, with the concentrations of 2.5, 1.3, 1.0, 0.5, 0.3, and 0.1 mg/L, respectively. These denatured albumin samples are pre-adsorbed on the gold surface on SPR. After the pre-adsorption, PBS rinses the surface to sweep excess weakly bound proteins to establish the baseline for the subsequent steps. Native albumin samples of 2 mg/mL flow across the pre-adsorbed surface. The SPR angle shift increases accordingly as the pre-adsorbed denatured albumins possess weaker affinity than the native ones so that they are replaced by the later ones via the competitive adsorption behavior. Upon rinsing with PBS, the SPR angle shift becomes stabilized to present the end of competitive adsorption behavior. By subtracting the baseline, SPR angle shifts at a given concentration of heavy metal ions are obtained, which are the function of the affinity difference between native and denatured proteins. The real time SPR sensorgram of the competitive adsorption process is shown in Figure 4.1.

4.3 Results and Discussion

Our SPR biosensor operates based upon the following two-step processes: first, Cu^{2+} ions interact with albumin, and then the interaction weakens the affinity of albumin to adsorb on a gold surface. Circular Dichroism (CD) and gold nanoparticle (AuNP) flocculation assay are adopted to visualize these two processes. The Cu^{2+}-denatured albumin is then pre-adsorbed on the gold surface and then native albumin flows to displace

47

the pre-adsorbed Cu^{2+}-denatured albumin. The sensitivity of SPR biosensor is characterized by different concentration of Cu^{2+} ions spiked in 4 different media, PBS, tap water, deionized water, and bottled water. 4 different heavy metal ions, Fe^{3+}, Mn^{2+}, Pb^{2+}, and Hg^{2+} are used to characterize the selectivity of the SPR biosensor, following the same protocol to characterize the sensitivity.

4.3.1 Characterization of the Competitive Adsorption Using Circular Dichroism (CD)

CD is a popular and powerful technique to study metal-protein interactions, which involves circular polarized light, such as the differential absorption of left- and right-handed light. Left-hand circular (LHC) and right-hand circular (RHC) polarized light present two possible spin angular momentum states for a photon. When circular polarized light passes through an absorbing optically active medium, the speeds between right and left polarization differ as well as their wavelength and the extent to which they are absorbed. The electric field of a light beam causes a linear displacement of charge when interacting with a molecule, whereas its magnetic field causes a circulation of charge. These two motions combined cause an excitation of an electron in a helical motion, which includes translation and rotation and their associated operators.

All specific secondary structures have their characteristic spectra (i.e., proteins with high contents of α-helices have characteristic bands at about 222 and 208 nm[79]). If Cu^{2+} ions induce conformational change, which only disrupt the tertiary structure but not the secondary structure, the characteristic bands will remain but vary CD angle shifts or band wavelengths (shown in Figure 4.2a).
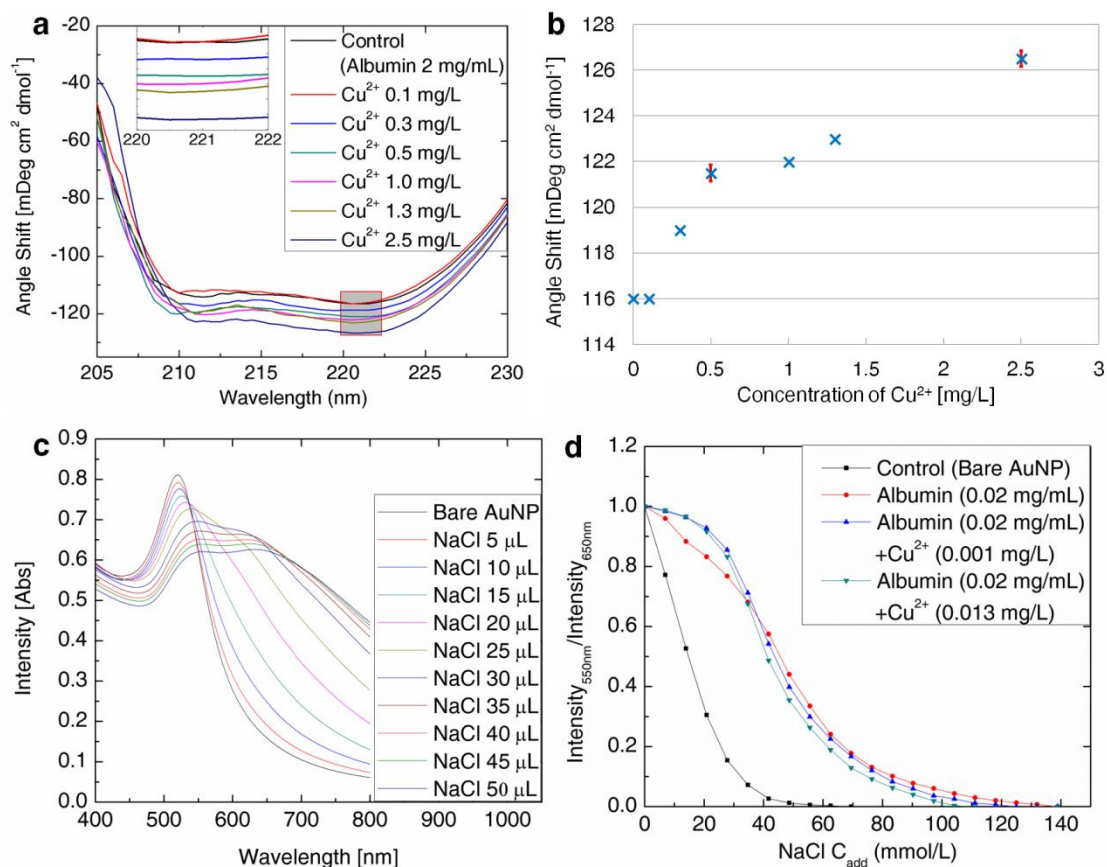
Figure 4.2 Circular Dichroism (CD) test and gold nanoparticle (AuNP) flocculation assay of albumin. **a.** the characteristic spectra change of α-helices in albumin with the concentration increasing of Cu^{2+}. Pure albumin with concentration of 2 mg/mL is used as the control. The red square shadow area (range of the wavelength from 220 to 222 nm) is enlarged as an inset. **b.** the intensity change of the characteristic band at 221 nm as a function of Cu^{2+} concentration. The red error bars indicate relative standard deviation (RSD). **c.** UV/Vis adsorption spectrum shows adsorption intensity as a function of wavelength at different NaCl titration concentrations. **d.** the ratio of the intensity at 550 nm to that at 650 nm as a function of titration concentrations: when no native, or denatured albumin, is added, bare AuNP (control) is readily titrated by NaCl, showing its curve at leftmost. Once native albumin is added, AuNPs are covered by albumin, consequently titration is obstructed. For instance, the ratio of 0.5 moves to rightmost, suggesting the affinity of native albumin to AuNPs is at maximum. As albumin is denatured by Cu^{2+}, the affinity of denatured albumin decreases, consequently moving the 0.5 ratio back to left.

We use Cu^{2+}-spiked albumin samples to perform the CD measurement. The characteristic bands, representing high contents of α-helices, are obtained at 221 and 210 nm, as shown in Figure 4.2a. As the higher concentrations of Cu^{2+} ions are spiked in

49

albumin samples, the CD angle shift increases (more negative) (in Figure 4.2b) while the characteristic spectra remain unchanged. This suggests that Cu^{2+} ions interact with albumin and the interaction is primarily on the tertiary structure of albumin, not on the secondary structure.

4.3.2   Characterization of Competitive Adsorption Using Gold Nanoparticle (AuNP) Flocculation Assay

The data from CD measurements support Cu^{2+} ions interact with albumin, yet they do not necessarily mean such interaction induces the affinity change on a gold surface. The characteristic spectra shown at CD measurements cannot be specifically linked to the affinity of albumin. We perform gold nanoparticle (AuNP) flocculation assay of albumin to observe the affinity change of albumin, caused by Cu^{2+} ions. AuNPs solution changes its color from pink to blue accompanied by the titration of NaCl. Added Na^+ and Cl^- reduce electrostatic repulsion of AuNPs so as to induce the aggregation of AuNPs. This aggregation changes the solution color that is decided by the size of AuNPs aggregates. If the AuNPs are fully surrounded by proteins, they are protected from the titration, resulting in no color change. The protection will be stronger if the interaction of AuNPs with proteins is stronger, so that higher concentration of added NaCl (C_{add} of NaCl) is needed to execute the titration. When the albumins are denatured by heavy metal ions, C_{add} of NaCl should be lower as the weaker affinity leading to the weaker protection.

Each set of titration generates a group of spectra. Taking bare AuNP solution for example (shown in Figure 4.2c), as titration continues, the peak at 550 nm becomes lower and broader, and moves to right, which represents the size of AuNPs aggregates becomes

more inhomogeneous. The formation of the new peak at 650 nm represents the final flocculation with larger size. The new peak is not sharp, suggesting inhomogeneous flocculation. Every set of scanning spectra in Figure 4.2c produces a data point in a curve in Figure 4.2d, through calculating the ratio of the intensity at 550 nm to that at 650 nm. All samples are diluted by 100 times to visualize the titration within 1000 milli-mol/L NaCl. Figure 4.2d illustrates the titration process with native albumin and denatured albumin as a function of Cu^{2+} concentration. The curve of bare AuNP is seen leftmost, indicating bare AuNP is readily titrated by NaCl. When native albumins are added to cover AuNPs, the high affinity native albumins obstruct titration so that high concentration of NaCl is needed to titrate at a given ratio of the spectra. Accordingly, the middle point (intensity ratio of 550 nm to 650 nm is 0.5) of this curve shifts to the rightmost. When AuNPs are covered by denatured albumin, the protection is weakened, so that curves' middle points return back to the left. The AuNP flocculation assay suggests that the affinity of albumin to a gold surface is indeed a function of the interaction of Cu^{2+} ions with albumin.

4.3.3 Detection of Cu^{2+} in Water Using SPR Biosensor

Ionic interactions, salt bridge between positively- and negatively-charged side chains, and disulfide bonds shape the conformation of albumins and manipulate the affinity of albumins to a sensing surface of SPR. The disrupted ionic interactions, caused by Cu^{2+} ions, result in less adsorption affinity to the sensing surface, which may be replaced by native albumins via competitive adsorption of proteins. Such affinity variation can be quantitatively measured in real time by SPR. This method offers very stable and consistent

SPR sensorgram as the SPR angle shift is generated by the replacement process rather than the adsorption process[58] as the displacement process is solely from the competition of two proteins (we have attempted to measure SPR angle shifts of Cu^{2+}-denatured albumin itself, yet the fluctuation of measurement largely compromises the accuracy of detection).
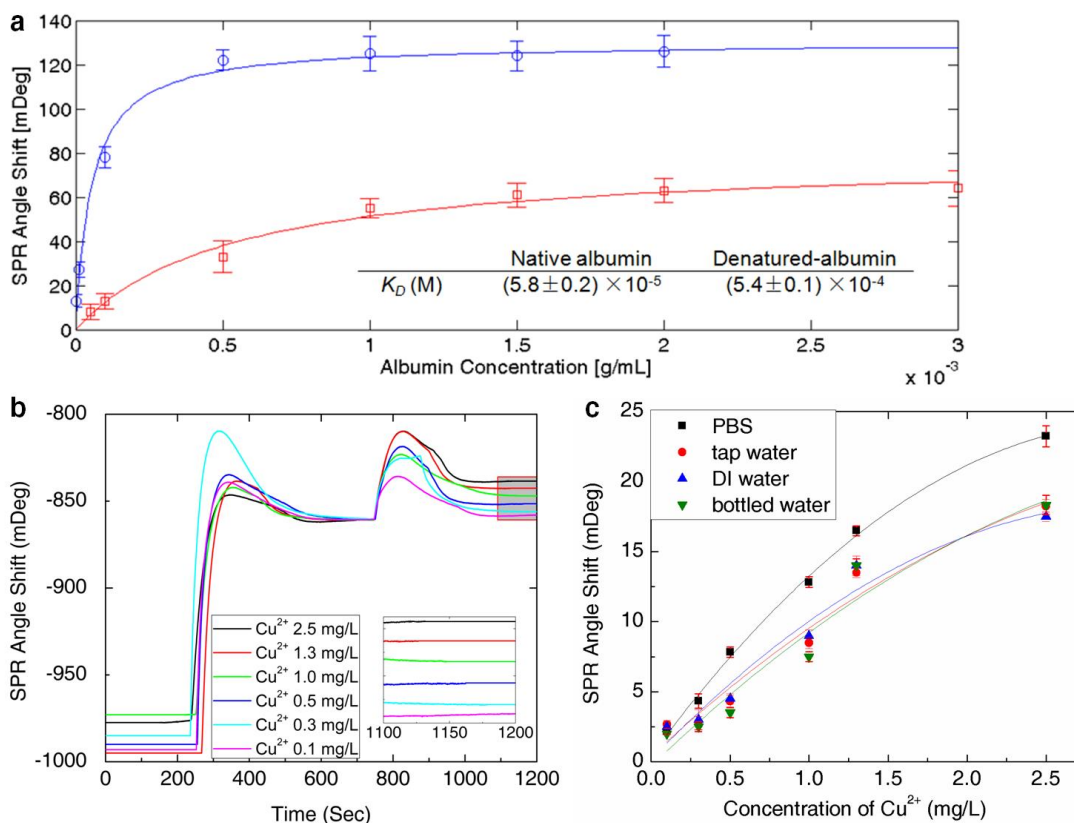

Figure 4.3 Sensitivity of SPR biosensor: **a.** SPR angle shift as a function of the concentrations of native (circular dots) and denatured albumin (square dots), and the dissociation constants (K_D) of native and denatured albumin on gold surface, calculated from the SPR angle shifts. **b.** SPR sensorgram, describing a series of displacements of denatured/native albumin in PBS as a function of Cu^{2+} concentration. The red square shadow area, between 1100 and 1200 sec, is enlarged as an inset. **c.** SPR angle shift as a function of Cu^{2+} concentration of 4 different liquid samples, including PBS, tap water, deionized (DI) water, and bottled water (Evian). As the concentration of Cu^{2+} increase, denatured albumins are replaced more easily, which generates larger SPR angle shift. The data points from tap water, DI water, and bottled water, produce similar outcomes, but quite distinct from those in PBS. Solid lines are polynomial fitted curves. The error bars indicate relative standard deviation (RSD).

In order to characterize the affinities of denatured albumin and native albumin, we measured K_D of denatured and native albumin using SPR (Figure 4.3a). One can calculate a dissociation constant from SPR angle shifts[45, 52]:

$$\Delta\theta = \Delta\theta_{max} C/(K_D + C)$$

$$4.1$$

$\Delta\theta$ is the SPR angle shift; $\Delta\theta_{max}$ is the SPR angle shift at the saturation; C is the heavy metal ions concentration; K_D is the dissociation constant.

K_D of native albumin is approximately one order of magnitude lower than that of denatured albumin, indicating the affinity of denatured albumin is far less than that of native albumin to gold surface, allowing the adsorption/desorption behavior of native/denatured albumin on SPR sensing surface.

Figure 4.3b and c shows SPR angle shifts increase as the concentration of Cu^{2+} increases. At the concentration of less than 1.0 mg/L, the polynomial fitted curves show relatively linear responses. The coefficient of determination, R^2 values of the lines are 0.9883, 0.9504, 0.9697, 0.9628 for PBS, tap water, deionized (DI) water, and bottled water, respectively. This linear characteristic agrees well with theoretical SPR angle shift, as shown in eq 4[79],

$$\Delta\theta(\lambda) = c_1\Delta n(\lambda) + c_2\Delta d$$

$$4.2$$

$\Delta\theta$ is SPR angle shift. Δn and Δd are changes in the refractive index and average thickness of an adsorbed molecular layer. λ is the wavelength of the incident light. c_1 and c_2 are constants.

Both Δn and Δd are strongly associated with the conformation characteristics and are directly correlated to the SPR angle shift. Moreover, Δn is linearly correlated with Δd, given in eq 5,

$$\Delta n = -\frac{1}{6n}\left(n^2+2\right)^2\left(\frac{n^2-1}{n^2+2}-\frac{n_w^2-1}{n_w^2+2}\frac{V_p}{V}\right)\frac{\Delta d}{d} \qquad 4.3$$

where n_w is the refractive index of water. n and d are refractive index and average thickness of an adsorbed molecular layer, respectively. V is the volume of the protein layer and is given by $V=V_p+V_w$, where V_p and V_w are the volumes of the proteins and water molecules in the layer, respectively. Therefore, SPR angle shift is theoretically linearly dependent on conformation change.

In Figure 4.3c, when the concentration is higher than 1.3 mg/L, SPR angle shift becomes nonlinear possibly due to the saturation of albumin denaturation. In a buffer (PBS), the SPR biosensor shows high sensitivity and the widest linear response region. We further promote the experiments under more realistic conditions, using tap water, DI water and bottled water (Evian). Data from these three samples show less sensitivity than those from PBS, and there is no obvious discrepancy among these data. The high sensitivity in PBS is because PBS contains more electrolytes that provide higher ionic strength to remain proteins' native conformations and behaviors.

4.3.4 Selectivity Characteristics of the SPR Biosensor

According to National Primary Drinking Water Regulations published by United States Environmental Protection Agency (EPA), the Maximum Contaminant Levels (MCL) of heavy metal ions in tap water include copper (1.3 mg/L), iron (0.3 mg/L),

manganese (0.05 mg/L), lead (0.015 mg/ L), and mercury (0.002 mg/L). The SPR biosensor is characterized by these 5 ions (Cu^{2+}, Fe^{3+}, Mn^{2+}, Pb^{2+}, and Hg^{2+}) for its selectivity as shown in Figure 4.4. Direct measurement of dissociation constants of albumin to heavy metal ions, using SPR, is a challenge. This is because the SPR angle is proportional to the refractive index change at the vicinity of the sensing surface which does not directly represent the interaction of albumin to heavy metal ions, but it represents the denatured albumin to the sensing surface through the pre-adsorption. Similar to Cu^{2+}, other 4 heavy metal ions, including Fe^{3+}, Mn^{2+}, Pb^{2+}, and Hg^{2+}, are bound to albumin and lower the affinity to gold surface. Higher concentration of the ions results in weaker affinity; thus the higher concentration of ions yields easier displacement by native albumin. In other words, the higher SPR angle shift of the displacement event represents weaker affinity of denatured albumin, which is consequently caused by higher concentration of the heavy metal ions. The dissociation constants of these heavy metal ions, Figure 4.4b, can be indirectly measured by a sequence of SPR angle shifts, similar to Cu^{2+}.
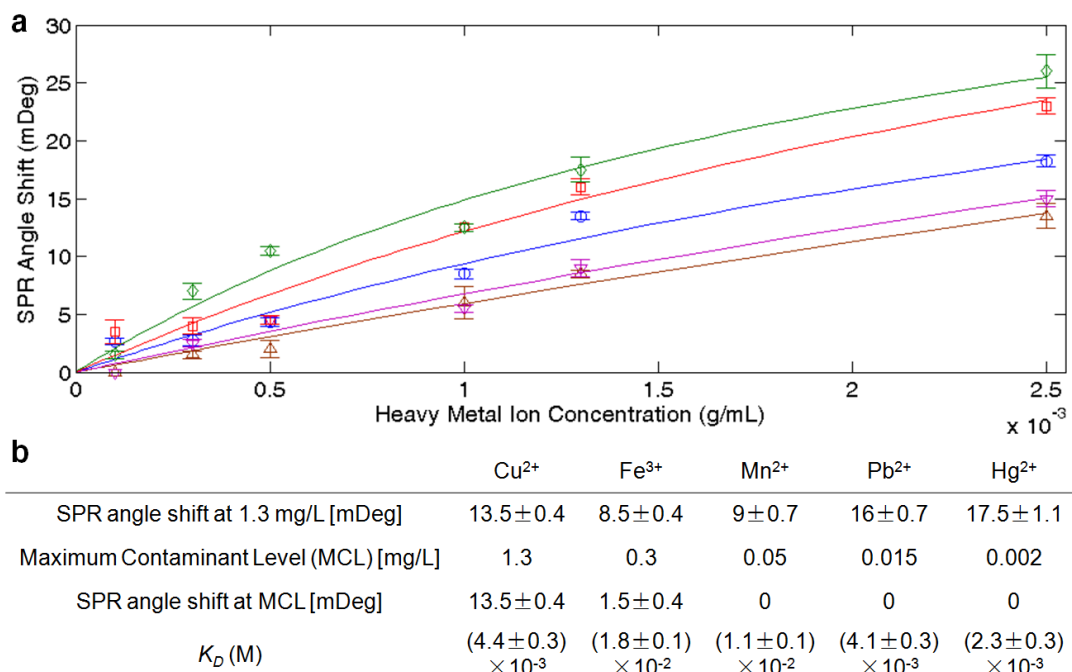
Figure 4.4 Selectivity of SPR biosensor. **a.** SPR angle shift as a function of heavy metal ion concentration: green diamond, red square, blue circle, purple lower-triangle, and brown upper-triangle dots/lines represent Hg^{2+}, Pb^{2+}, Cu^{2+}, Mn^{2+}, Fe^{3+}, respectively. The error bars indicate relative standard deviation (RSD). **b.** SPR angle shifts at the concentration of 1.3 mg/L and the Maximum Contaminant Levels (MCL) in tap water, and K_D of various heavy metal ions. K_D is correlated to the dissociation constants of heavy metal ions to albumin.

We set a concentration of all heavy metal ions at 1.3 mg/L, MCL of Cu^{2+}, and performed SPR measurements of a sequence of pre-adsorbing denatured albumin, PBS wash, replacing the pre-adsorbed albumin by native albumin, and PBS wash, following the same protocol we used to characterize the SPR biosensor for Cu^{2+}. The SPR angle shifts of Fe^{3+}, Mn^{2+}, Pb^{2+}, and Hg^{2+}, were 8.5, 9, 16, and 17.5, respectively. As expected, the heavy metal ions denature albumin and result in SPR angle shift. The sensitivity to these heavy metal ions at 1.3 mg/L varies, yet it is not very distinctive. Then we measured the SPR angle shift of these ions at their respective MCL (Fe^{3+}: 0.3 mg/L, Mn^{2+}: 0.05 mg/L, Pb^{2+}:

0.015 mg/L, and Hg^{2+}: 0.002 mg/L) and the SPR angle shifts of Fe^{3+}, Mn^{2+}, Pb^{2+}, Hg^{2+} were 1.5, 0, 0, 0 mDeg, respectively, which are significantly less than that of Cu^{2+}, 13.5 mDeg, at 1.3 mg/L (MCL of Cu^{2+}).

These data suggest both the limitation and application of our SPR biosensor. The SPR biosensor in general has the lack of selectivity to different heavy metal ions. Heavy metal ions do result in conformational changes and denaturation of albumin, resulting in SPR angle shifts. On the other hand, the SPR biosensor serves well in tap water samples to detect Cu^{2+} as the most serious threat in tap water is Cu^{2+} and the SPR responses at MCL of other heavy metal ions are significantly less than that of Cu^{2+}.

CHAPTER 5

SUMMARY AND SIGNIFICANCE

In the first project of this dissertation, a reusable SPR biosensor was developed to detect the fibrinogen concentration in undiluted human serum. The surface of the biosensor chip was regenerated for reuse by bleach, which reduces batch-to-batch irreproducibility and uncontrollable experimental conditions, which generates unalterable false-positive/negative responses. Using the competitive adsorption/exchange nature of proteins along with a regeneration procedure, this SPR biosensor provides a label-free and high throughput measurement technique for fibrinogen of multiple samples in real time. From our experiments, it was demonstrated that the concentration levels could be differentiated in the range of 0.5 to 2.5 mg/mL.

In the second project, a SPR biosensor using the competitive adsorption of proteins (the Vroman effect) and pattern recognition is demonstrated to detect Tg in undiluted human serum. Based on cross-responses, the biosensor bypasses the need of specific capture of the target analyte, Tg, and enhances the selectivity to discriminate the tiny discrepancies among multiple samples. Through the analysis of LDA, explicit plots and quantitative indices are generated from the composite patterns. At last, we successfully detect Tg with 100 ng/mL, 10 ng/mL and 2 ng/mL in undiluted human serum, and estimate the possibility to predict the classification of a Tg sample with an unknown concentration.

In the last project, SPR is used to detect Cu^{2+}, a common contaminant in tap water, using competitive adsorption of proteins, termed Vroman effect. Cu^{2+}-denatured albumin has lower affinity than native albumin to gold surface, which can be replaced by a sequence

of adsorption/desorption phenomena. This sequence of adsorption/desorption is monitored by SPR in real time to quantify the concentration of Cu^{2+} ions in water samples, including PBS, tap water, DI water, and bottled water. The affinity change of protein denaturation by Cu^{2+} is demonstrated by Circular Dichroism and gold nanoparticle (AuNP) flocculation assay. The SPR biosensor can detect down to 0.1 mg/L Cu^{2+}, lower than the Maximum Contaminant Level (MCL), 1.3 mg/L, in National Primary Drinking Water Regulations published by United States Environment Protection Agency (EPA). The SPR biosensor is characterized for 5 different heavy metal ions, Cu^{2+}, Fe^{3+}, Mn^{2+}, Pb^{2+}, Hg^{2+}, for its selectivity. At MCL, the SPR biosensor produces 13.5 ± 0.4, 1.5 ± 0.4, 0, 0, 0 mDeg, respectively, suggesting the biosensor may be used to detect Cu^{2+} in tap water samples. Such technique may complement existing biosensors to add a sensing modality to facilitate the heavy metal ions detection.

References

[1] Higgins, I.J., Lowe, C.R., 1987. Introduction to the principles and applications of biosensors. Philos. Tans. R. Soc. Lond. B Biol. Sci. 316(1176), 3-11.

[2] Choi, S., Yang, Y., Chae, J., 2008. Surface plasmon resonance protein sensor using Vroman effect. Biosens. Bioelectron. 24(4), 893-899.

[3] Haab, B.B., 2003. Methods and applications of antibody microarrays in cancer research. Proteomics 3(11), 2116-2122.

[4] Yu, X., Xu, D., Cheng, Q., 2006. Label-free detection methods for protein microarrays. Proteomics 6(20), 5494-5503.

[5] Bally, M., Halter, M., Vörös, J., Grandin, H.M., 2006. Optical microarray biosensing techniques. Surf. Interface. Anal. 38(11), 1442-1458.

[6] Chaerkady, R., Pandey, A., 2008. Applications of proteomics to lab diagnosis. Annu. Rev. Pathol. Mech. Dis. 3, 485-489.

[7] Choi, S., Wang, R., Lajevardi-Khosh, A., Chae, J., 2010. Using competitive protein adsorption to measure fibrinogen in undiluted human serum. Appl. Phys. Lett. 97(25), 253701.

[8] Frederix, F. et al., 2004. Reduced nonspecific adsorption on covalently immobilized protein surfaces using poly(ethylene oxide) containing blocking agents. J. Biochem. Biophys. Methods 58(1), 67-74.

[9] Daniels, J.S., Pourmand, N., 2007. Label-free impedance biosensor: opportunities and challenges. Electroanal. 19(12), 1239-1257.

[10] Vroman, L., Adams, A.L., 1969. Findings with the recording ellipsometer suggesting rapid exchange of specific plasma proteins at liquid/solid interfaces. Surf. Sci. 16, 438-446.

[11] Jung, S.Y. et al., 2003. The Vroman effect: a molecular level description of fibrinogen displacement. J. Am. Chem. Soc. 125(42), 12782-12786.

[12] Willems, G.M., Hermens, W.T., Hemker, H.C., 1991. Surface exclusion and molecular mobility may explain Vroman effects in protein adsorption. J. Biomater. Sci. Polym. Ed. 2(3), 217-226.

[13] Turbill, P., Beugeling, T., Poot, A.A., 1996. Proteins involved in the Vroman effect during exposure of human blood plasma to glass and polyethylene. Biomaterials 17(13), 1279-1287.

[14] Krishnan, A., Siedlecki, C.A., Vogler, E.A., 2004. Mixology of protein solution and the Vroman effect. Langmuir 20(12), 5071-5078.

[15] Noh H., Vogler, E.A., 2007. Volumetric interpretation of protein adsorption: competition from mixtures and the Vroman effect. Biomaterials 28(3), 405-422.

[16] Slack, S.M., Horbett, T.A., 1989. Changes in the strength of fibrinogen attachment to solid surface: an explanation of the influence of surface chemistry on the Vroman effect. J. Colloid Interf. Sci. 133(1), 148-165.

[17] Leonard, E.F., Vroman, L., 1992. Is the Vroman effect of importance in the interaction of blood with artificial materials? J. Biomater. Sci. Polym. Ed. 3(1), 95-107.

[18] Choi, S., Chae, J., 2010. Methods of reducing non-specific adsorption in microfluidic biosensors. J. Micromech. Microeng. 20(7), 075015.

[19] De, M. et al., 2009. Sensing of proteins in human serum using nanoparticle-green fluorescent protein conjugates. Nature Chem. 1(6), 461-465.

[20] Sahab, Z.J., Semaan, S.M., Sang, Q.X.A., 2007. Methodology and applications of disease biomarker identification in human serum. Biomark. Insights 2, 21-43.

[21] Pulido, R., Huijsduijnen, R.H.V., 2008. Protein tyrosine phosphatases: dual-specificity phosphatases in health and disease. FEBS J. 275(5), 848-866.

[22] Darwish, I.A., Blake, D.A., 2002. Development and validation of a one-step immunoassay for determination of cadmium in human serum. Anal. Chem. 74(1), 52-58.

[23] Beveridge, T.J. et al., 1996. Metal-microbe interactions: contemporary approaches. Adv. Microb. Physiol. 38, 177-243.

[24] Bontidean, I. et al., 2000. Bacterial metal-resistance proteins and their use in biosensors for the detection of bioavailable heavy metals. J. Inorg. Biochem. 79(1-4), 225-229.

[25] Bontidean, I. et al., 1998. Detection of heavy metal ions at femtomolar levels using proteins-based biosensor. Anal. Chem. 70(19), 4162-4169.

[26] Shankaran, D.R., Miura, N., 2007. Trends in interfacial design for surface plasmon resonance based immunoassays. J. Phys. D Appl. Phys. 40(23), 7187-7200.

[27] Wu, J., Fu, Z., Yan, F., Ju, H., 2007. Biomedical and clinical applications of immunoassays and immunosensors for tumor markers. Trends Anal. Chem. 26(7), 679-688.

[28] Latour Jr, R.A., 2005. Biomaterials: protein-surface interactions, in Bowlin, G.L., Wnek, G.E. (Eds.), Encyclopedia of Biomaterials and Biomedical Engineering. Taylor & Francis, New York, pp. 1-15.

[29]Elwing, H., Askendal, A., Lundström, I., 1987. Competition between adsorbed fibrinogen and high molecular weight kininogen on solid surface incubated in human plasma (the Vroman effect): influence of solid surface wettability. J. Biomed. Mater. Res. 21(8), 1023-1028.

[30] Poot, A., Beugeling, T., Van Aken, W.G., Bantjes, A., 1990. Detection of surface-adsorbed (lipo)proteins by means of a two-step enzyme-immunoassay: A study of the Vroman effect. J. Biomed. Mater. Res. 24(8), 1021-1036.

[31] Wang, R., Lajevardi-Khosh, A., Choi, S., Chae, J., 2011. Regenerative Surface Plasmon Resonance (SPR) biosensor: real-time measurement of fibrinogen in undiluted human serum using the competitive adsorption of proteins. Biosens. Bioelectron. 28(1), 304-307.

[32] Ince, R., Narayanaswamy, R., 2006. Analysis of the performance of interferometry, surface plasmon resonance and luminescence as biosensors and chemosensors. Anal. Chim. Acta. 569(1-2), 1-20.

[33] Li, Y.J., Xiang, J., Zhou, F., 2007. Sensitive and label-free detection of DNA by surface plasmon resonance. Plasmonics 2(2), 79-87.

[34] Moré, S.D., Hudecek, J., Urisu, T., 2003. Hydrophobic/hydrophilic interactions of cytochrome c with functionalized self-assembled monolayers on silicon. Surf. Sci. 532-535, 993-998.

[35] Meade, T.W. et al., 1986. Haemostatic function and ischaemic heart disease: principal results of the Northwick Park Heart Study. Lancet 328(8506), 533-537.

[36] Wilhelmsen, L. et al., 1984. Fibrinogen as a risk factor for stroke and myocardial infarction. New Engl. J. Med. 311(8), 501-505.

[37] Nieuwenhuizen, W., 1995. Biochemistry and measurement of fibrinogen. Eur. Heart J. 16, 6-10.

[38] Kamath, S., Lip, G.Y., 2003. Fibrinogen: biochemistry, epidemiology and determinants. QJM. 96(10), 711-729.

[39] Asanov, A.N., Wilson, W.W., Oldham, P.B., 1998. Regenerable biosensor platform: a total internal reflection fluorescence cell with electrochemical control. Anal. Chem. 70(6), 1156–1163.

[40] Choi, S., Chae, J., 2009. A regenerative biosensing surface in microfluidics using electrochemical desorption of short-chain self-assembled monolayer. Microfluid. Nanofluid. 7(6), 819-827.

[41] Duren, M. et al., 1999. Value of stimulated serum thyroglobulin levels for detecting persistent or recurrent differentiated thyroid cancer in high- and low-risk patients. Surgery 126(1), 13-19.

[42] Aizawa, T. et al., 1990. Serum thyroglobulin concentration as an indicator for assessing thyroid stimulation in patients with Graves' disease during antithyroid drug therapy. Am. J. Med. 89(2), 175-180.

[43] Voller, A., Bartlett, A., Bidwell, D.E., 1978. Enzyme immunoassays with special reference to ELISA techniques. J. Clin. Pathol. 31(6), 507-520.

[44] Stanley, M.D., Goldsmith, J., 1975. Radioimmunoassay: Review of basic principles. Semin. Nucl. Med. 5(2), 125-152.

[45] Wright, A.T., Anslyn, E.V., 2005. Differential receptor arrays and assays for solution-based molecular recognition. Chem. Soc. Rev. 35(1), 14-28.

[46] Lavigne, J.J., Anslyn, E.V., 2001. Sensing a paradigm shift in the field of molecular recognition: from selective to differential receptors. Angew. Chem. Int. Ed. 40(17), 3118-3130.

[47] Choi, S., Huang, S., Li, J., Chae, J., 2011. Monitoring protein distributions based on patterns generated by protein adsorption behavior in a microfluidic channel. Lab Chip 11(21), 3681-3688.

[48] Zhou, H., Baldini, L., Hong, J., Wilson, A.J., Hamilton, A.D., 2006. Pattern recognition of proteins based on an array of functionalized porphyrins. J. Am. Chem. Soc. 128(7), 2421-2425.

[49] Gouma, P., Sberveglieri, G., 2004. Novel materials and applications of electronic noses and tongues. Mater. Res. Soc. 29(10), 697-702.

[50] Suslick, K.S., 2004. An optoelectronic nose: "seeing" smells by means of colorimetric sensor arrays. Mater. Res. Soc. 29(10), 720-725.

[51] Freund, M.S., Lewis, N.S., 1995. A chemically diverse conducting polymer-based "electronic nose". Proc. Natl. Acad. Sci. 92(7), 2652-2656.

[52] Latour Jr, R.A., Hench, L.L., 2002. A theoretical analysis of the thermodynamic contributions for the adsorption of individual protein residues on functionalized surfaces. Biomaterials 23(23), 4633-4648.

[53] Forzani, E.S., Zhang, H., Chen, W., Tao, N., 2005. Detection of heavy metal ions in drinking water using a high-resolution differential surface plasmon resonance sensor. Environ. Sci. Technol. 39(5), 1257-1262.

[54] Forzani, E.S., Foley, K., Westerhoff, P., Tao, N., 2007. Detection of arsenic in groundwater using a surface plasmon resonance sensor. Sensor Actuat. B-Chem. 123(1), 82-88.

[55] Brewer, G.J., 2010. Copper toxicity in the general population. Clin. Neurophysiol. 121(4), 459-460.

[56] Bannon, D.I., Chisolm Jr, J.J., 2001. Anodic stripping voltammetry compared with graphite furnace atomic absorption spectrophotometry for blood lead analysis. Clin. Chem. 47(9), 1703-1704.

[57] Liu, H.W., Jiang, S.J., Liu, S.H., 1999. Determination of cadmium, mercury and lead in seawater by electrothermal vaporization isotope dilution inductively coupled plasma mass spectrometry. Spectrochim. Acta. B 54(9), 1367-1375.

[58] Yang, W., Chow, E., Willett, G.D., Hibbert, D.B., Gooding, J.J., 2003. Exploring the use of the tripeptide Gly-Gly-His as a selective recognition element for the fabrication of electrochemical copper sensors. Analyst 128(6), 712-718.

[59] Baldo, M.A., Daniele, S., Ciani, I., Bragato, C., Wang, J., 2004. Remote stripping analysis of lead and copper by a mercury-coated platinum microelectrode. Electroanal. 16(5), 360- 366.

[60] Eksperiandova, L., Blank, A.B., Makarovskaya, Y.N., 2002. Analysis of waste water by X-ray fluorescence spectrometry. X-ray Spectrom. 31(3), 259-263.

[61] Arai, Y., Lanzirotti, A., Sutton, S., Davis, J.A., Sparks, D.L., 2003. Arsenic speciation and reactivity in poultry litter. Environ. Sci. Technol. 37(18), 4083-4090.

[62] Sonthalia, P., McGaw, E., Show, Y., Swain, G.M., 2004. Metal ion analysis in contaminated water samples using anodic stripping voltammetry and a nanocrystalline diamond thin-film electrode. Analytica. Chimica. Acta. 522(1), 35-44.

[63] Farghaly, O.A., Ghandour, M.A., 2005. Square-wave stripping voltammetry for direct determination of eight heavy metals in soil and indoor-airborne particular matter. Environ. Res. 97(3),229-235.

[64] Wang, S., Forzani, E.S., Tao, N., 2007. Detection of heavy ion in water by high-resolution surface plasmon resonance spectroscopy combined with anodic stripping voltammetry. Anal. Chem. 79(12), 4427-4432.

[65] Burdette, S.C., Frederickson, C.J., Bu, W., Lippard, S.J., 2003. ZP4, an improved neuronal Zn^{2+} sensor of the Zinpyr family. J. Am. Chem. Soc. 125(7), 1778-1787.

[66] Wu, X.Q., Kim, J., Dordick, J.S., 2000. Enzymatically and combinatorially generated array-based polyphenol metal ion sensor. Biotechnol. Prog. 16(3), 513-516.

[67] Shetty, R.S. et al., 2003. Luminescence-based whole-cell-sensing systems for cadmium and lead using genetically engineered bacteria. Anal. Bioanal. Chem. 376(1), 11-17.

[68] Deo, S., Godwin, H.A., 2000. Aselective, ratiometric fluorescent sensor for Pb^{2+}. J. Am. Chem. Soc. 122(1), 174-175.

[69] Yang, W.R. et al., 2001. Sub-ppt detection limits for copper ions with Gly-Gly-His modified electrodes. Chem. Commun. 19, 1982-1983.

[70] Shults, M.D., Pearce, D.A., Imperiali, B., 2003. Modular and tunable chemosensor scaffold for divalent zinc. J. Am. Chem. Soc. 125(35), 10591-10597.

[71] Mlynarz, P. et al., 2002. Impact of the peptide sequence on the coordination abilities of albumin-like tripeptides towards Cu^{2+}, Ni^{2+} and Zn^{2+} ions. Potential albumin-like peptide chelators. New J. Chem. 26(2), 264-268.

[72] Lu, Y. et al., 2003. New highly sensitive and selective catalytic DNA biosensors for metal ions. Biosens. Bioelectron. 18(5-6), 529-540.

[73] Rouch, D.A., Parkhill, J., Brown, N.L., 1995. Induction of bacterial mercury- and copper-responsive promoters: functional differences between inducible systems and implications for their use in gene-fusions for in vivo metal biosensors. J. Ind. Microbiol. 14(3-4), 349-353.

[74] Sharma, S.K., Goloubinoff, P., Christen, P., 2008. Heavy metal ions are potent inhibitors of protein folding. Biochem. Bioph. Res. Co. 372(2), 341-345.

[75] Renwrantz, L., Werner, I., 2008. Origin of a metal-binding protein in serum of mytilus edulis. J. Mollus. Stud. 74(1), 11-17.

[76] Capanni, C. et al., 2004. Investigation of the effects of copper ions on protein aggregation using a model system. Cell. Mol. Life Sci. 61(7-8), 982-991.

[77] Hoefling, M., Monti, S., Corni, S., Gottschalk, K.E., 2011. Interaction of β-sheet folds with a gold surface. PLoS One 6(6), e20925.

[78] Boujday, S. et al., 2008. In-depth investigation of protein adsorption on gold surfaces: correlating the structure and density to the efficiency of the sensing layer. J. Phys. Chem. B 112(21), 6708-6715.

[79] Boussaad, S., Pean, J., Tao, N.J., 2000. High-resolution multiwavelength surface plasmon resonance spectroscopy for probing conformational and electronic changes in redox proteins. Anal. Chem. 72(1), 222-226.